



HAL
open science

Influence Of Bottom Topography On An Upwelling Current: Generation Of Long Trapped Filaments

T. Meunier, V. Rossi, Y. Morel, X. Carton

► **To cite this version:**

T. Meunier, V. Rossi, Y. Morel, X. Carton. Influence Of Bottom Topography On An Upwelling Current: Generation Of Long Trapped Filaments. *Ocean Modelling*, 2010, 35 (4), pp.277-303. <10.1016/j.ocemod.2010.08.004>. <hal-00998661>

HAL Id: hal-00998661

<https://hal.science/hal-00998661v1>

Submitted on 4 Jun 2014

HAL is a multi-disciplinary open access archive for the deposit and dissemination of scientific research documents, whether they are published or not. The documents may come from teaching and research institutions in France or abroad, or from public or private research centers.

L'archive ouverte pluridisciplinaire **HAL**, est destinée au dépôt et à la diffusion de documents scientifiques de niveau recherche, publiés ou non, émanant des établissements d'enseignement et de recherche français ou étrangers, des laboratoires publics ou privés.



HAL Authorization

Influence of bottom topography on an upwelling current : generation of long trapped filaments

T. Meunier^{*,a}, V. Rossi^b, Y. Morel^c, X. Carton^a

^aLaboratoire de Physique de l'Océan, Université de Bretagne Occidentale, 46 avenue Legorgeu, 29200 Brest, France

^bLaboratoire d'Études en Géophysique et Océanographie Spatiale, CNRS, Observatoire Midi-Pyrénées, 14 avenue Edouard Belin, 31400 Toulouse, France

^cService hydrographique et océanographique de la marine, (SHOM), 42 av Gaspard Coriolis, 31057 Toulouse, France

Abstract

We investigate the influence of bottom topography on the formation and trapping of long upwelling filaments. They use a 2-layer shallow water model on the f-plane. A wind forced along-shore current, associated with coastal upwelling along a vertical wall, encounters a promontory of finite width and length, perpendicular to the coast.

In the lower layer, topographic eddies form, which are shown to drive the formation of a filament on the front. Indeed, as the upwelling current and front develop along the coast, the along shore flow crosses the promontory, re-arranging the potential vorticity structure and generating intense vortical structures : water columns with high potential vorticity initially localized upon the promontory are advected into the deep ocean, forming cyclonic eddies, while water columns from the deep ocean with low potential vorticity climb on the topography forming a trapped anti-cyclonic circulation. These topographic eddies interact with the upper layer upwelling front and form an elongated, trapped and narrow filament.

Sensitivity tests are then carried out and it is shown that :

- baroclinic instability of the front does not play a major role on the formation of long trapped filaments;
- increasing the duration of the wind forcing increases the upwelling current and limits the offshore growth of the filament;
- modifying the promontory characteristics (width, length, height and slopes) has strong impact on the filament evolution, sometimes leading to a multipolarisation of the potential vorticity anomaly structure which results in much more complicated patterns in the upper layer (numerous shorter and less coherent filaments). This shows that only specific promontory shapes can lead to the formation of well defined filaments;
- adding bottom friction introduces a slight generation of potential vorticity in the bottom layer over the promontory, but does not significantly alter significantly the formation of the filament along the outcropped front in the present configuration;
- modifying the stratification characteristics, in particular the density jump between the layers, has only a weak influence on the dynamics of topographic eddies and on filament formation;

- the influence of capes is also modest in our simulations, showing that topography plays the major role in the formation of long and trapped upwelling filaments.

Key words: Eastern boundary, Mesoscale dynamics, Upwelling/Downwelling, Topographic flows, Upwelling filaments, Potential vorticity

1 Introduction

Long trapped filaments of cold water are ubiquitous features along upwelling fronts. They sometimes extend hundreds of kilometers offshore and have been shown to play a major role in the offshore transport of recently upwelled coastal water ([Kostianoy and Zatsepin, 1996]) and in feeding the oligotrophic offshore waters with nutrients and organic materials ([Alvarez-Salgado *et al.*, 2007] and more particularly over the Iberian peninsula upwelling [Alvarez-Salgado *et al.*, 2001]). They are thus important physical features for eastern boundary upwelling ecosystems.

Figure 1 shows a set of satellite images of the Iberian peninsula on the 09/05/2009 (column 1) and 09/05/2005 (column 2).. The images on the first row are the Sea Surface Temperature (SST) and on the second row the Chlorophyll-a concentration (Sea Surface Color). Long, trapped and recurrent filaments are observed on SST and chlorophyll maps off Cape Finisterre (43°N), São Vicente (37°N) and the Estremadura promontory (between 38.5 and 39.5°N). However on all maps, another tongue of cold upwelled water pointing offshore also clearly arises from the upwelling front just South of the Estremadura promontory.

In-situ and remotely sensed data have provided some descriptions of upwelling filaments (see for instance [Brink, 1983]; [Flament *et al.*, 1985]; [Washburn and Armi, 1988]; [Strub *et al.*, 1991]; [Navarro-Pérez and Barton, 1998]; [Barton, 2001]), and many numerical and theoretical studies have focused on their dynamics. [Haynes *et al.*, 1993] used satellite data of the West-Iberia upwelling system to show that large filaments were often closely related with capes, but noted the repeated occurrence of two large filaments at two different locations corresponding with a straight coastline. They assumed that those filaments were related with unstable meanders of the jet, but their stationarity remained unexplained.

One of the first process studies on upwelling filament dynamics was performed by [Haidvogel *et al.*, 1991]. Their model was able to reproduce cold filaments along the upwelling front. They concluded from a set of sensitivity cases, including removal of the coastline geometry and the bottom topography, that the presence of large capes along the coast, was necessary to the generation of upwelling filaments. [Marchesiello *et al.*, 2003] studied the equilibrium structure of the California current system and conducted different sensitivity tests. They showed that mesoscale variability was intrinsic to the current and not due to the variability of the forcing. Contrary to [Haidvogel *et al.*, 1991], they showed that even in the case of a straight coastline and a flat bottom, upwelling filaments and eddies still occurred, but with no preferential location, confirming the conclusions of [Roed and Shi, 1999], that instability induced filaments and eddies could happen in the absence of coastal irregularities. Removing only the topography,

*Corresponding author

Email addresses: thomas.meunier@univ-brest.fr (T. Meunier), vincent.rossi@legos.obs-mip.fr (V. Rossi), yves.morel@shom.fr (Y. Morel), xavier.carton@univ-brest.fr (X. Carton)

Preprint submitted to Ocean Modelling

June 3, 2014

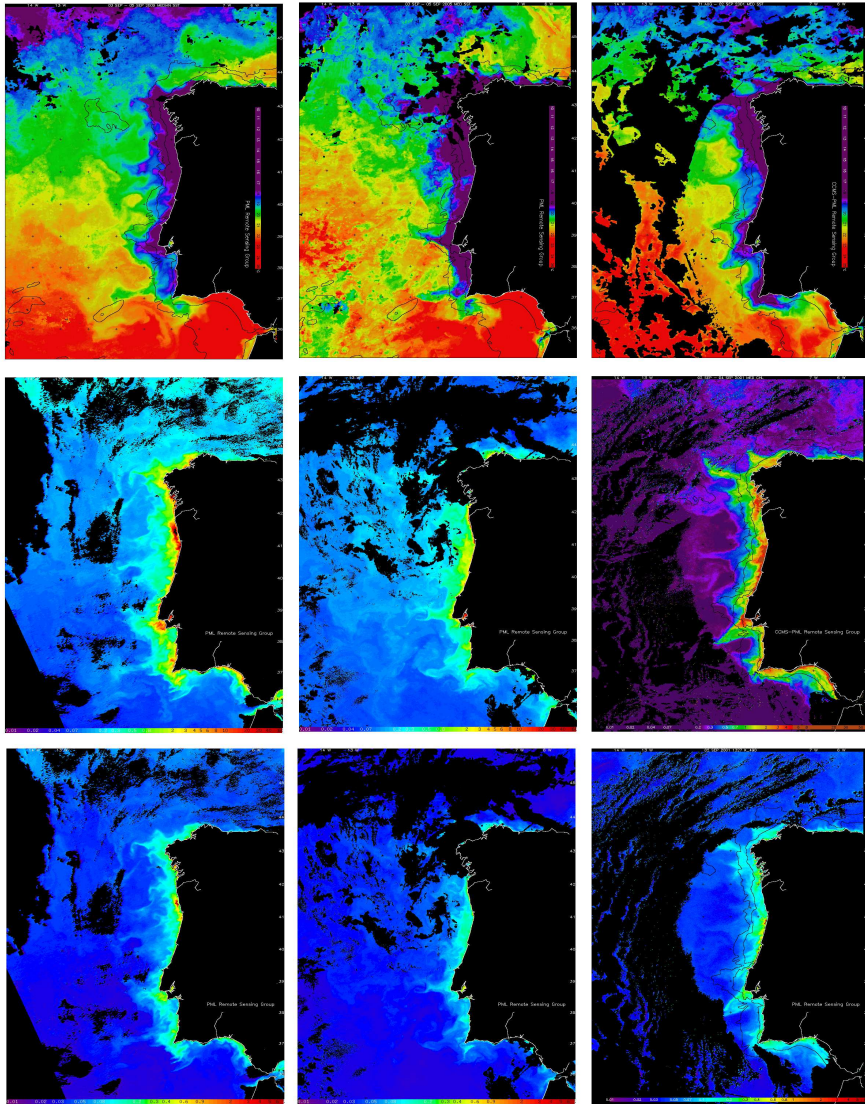


Figure 1: Sea Surface Temperature (first column) and Chlorophyll distribution (second column) situation off the West Iberian coast during three distinct upwelling episodes (04/09/2005 on the first row and 05/09/2009 on the second row.)

35 [Marchesiello *et al.*, 2003] concluded that a standing wave could be generated at the cape, in
36 agreement with results from a numerical study of [Batteen, 1997] who noted anchoring of
37 filaments at coastline irregularities, while [Roed and Shi, 1999] only noted a weak anchoring of
38 the meander. [Ikeda, 1981] and [Ikeda, 1989] showed using two-layer quasigeostrophic models,
39 that unstable meanders of a buoyancy driven coastal jet would move downstream by a combined
40 effect of propagation and advection, so that some physical process had to be involved in the
41 anchoring of filaments at the capes as observed by [Marchesiello *et al.*, 2003].

42 Recently [Batteen *et al.*, 2007] conducted a process oriented study of the Northern Canary
43 Current System (NCCS) and revisited the upwelling instability and filamentation problem in this
44 region. They modified the bottom topography, boundary conditions and wind forcing and found
45 that :

- 46 • the flat bottom experiment shows many of the typically observed features of the NCCS;
- 47 • adding the bottom topography shows that topography has an important role in intensifying
48 and trapping the equatorward current near the coast, in weakening the subsurface poleward
49 current, and in intensifying eddies off the capes of Iberia;
- 50 • the flat bottom experiment produces anticyclonic meanders near cabo Roca and Cabo São
51 Vincente, but not off Figueira da Foz;
- 52 • the beta effect plays an important role on the formation of the subsurface meander off cabo
53 Roca.

54 To summarize, four main source have been identified to explain the generation of filaments
55 along upwelling fronts :

- 56 • the frontal or baroclinic instability of the front;
- 57 • the effect of capes;
- 58 • the planetary beta effect;
- 59 • bottom topography.

60 Upwelling filaments have also been classified into different types (see [Strub *et al.*, 1991]), but
61 one important distinction is whether they are trapped or not. Because the trapping of filaments
62 always happens at the same locations, we believe that the observed long trapped upwelling fil-
63 aments are associated with topographic features and we chose to focus on this aspect in the
64 present study. Again, different studies ([Ikeda, 1989, Capet and Carton, 2004]) concluded that
65 topographic irregularities were destabilization source for upwelling fronts, but the effect of bot-
66 tom topography on the development of trapped filaments has not received a lot of attention, in
67 particular the details of the mechanism is not clear and its sensitivity to different parameters
68 remains to be studied.

69 [Stern and Chassignet, 2000] showed, using both a $1_{1/2}$ and a three-layer isopycnic model,
70 that intrinsic instability was not sufficient to generate detrainment of fluid and eddy-separation
71 from the jet. They concluded that, to generate a blocking wave and detrain water, there was
72 a need for a downstream variation in jet transport, and noted that this variation could happen
73 in the case of alongshore varying topography, but did not investigate further on this point.
74 [Viera and Grimshaw, 1994] studied the evolution of a potential vorticity front over an iso-
75 lated topography, using a $1_{1/2}$ layers quasi-geostrophic model, and showed, that a linearly

76 stable jet associated with a potential vorticity front could produce large and pinched off me-
 77 anders when interacting with bottom topography. [Herbette et al., 2003] have shown that a
 78 seamount could interact with a surface intensified eddy and generate filaments (or even split
 79 the eddy). Finally, while studying the generation of secondary upwelling fronts along continen-
 80 tal slopes [Rossi et al., 2009] found, in one of the experiment with a promontory (see fig. 22 in
 81 [Rossi et al., 2009]), that a bottom topography could trap upwelled waters and even observed the
 82 formation of a trapped filament extending offshore.

83 Therefore, we study the evolution of an upwelling front in the presence of an along shore
 84 varying topography, in the form of cross-shore coastal promontories. We focus on the formation
 85 and trapping of long filaments extending offshore and we base our approach on the potential
 86 vorticity analysis used in the papers quoted in the previous paragraph.

87 The outline is :

- 88 • in section 2 (Model and tools) we describe the numerical model and recall some basic princi-
 89 ples relating potential vorticity (thereafter *PV*) and potential vorticity anomalies (thereafter
 90 *PVA*) to the dynamics;
- 91 • in section 3 (Reference experiment) we present a first simulation that illustrates the devel-
 92 opment of a long filament. In particular we describe how the generation of *PVA* by the
 93 displacement of water columns above the promontory can generate a permanent filament
 94 trapped downstream of the promontory;
- 95 • in section 4 (Sensitivity study) we study the sensitivity of this mechanism to different
 96 regimes and parameters : stable and unstable cases, wind forcing duration, promontory
 97 height, width and length, stratification, bottom friction;
- 98 • in section 5 (Conclusion) we sum up and discuss our results.

99 2. Model and tools

100 2.1. Equations and model

101 The model used is an adiabatic version of MICOM (Miami Isopycnic Coordinate Ocean
 102 Model) ([Bleck and Boudra, 1986]; [Bleck and Smith, 1990];[Bleck et al., 1992]) modified to
 103 include a fourth order scheme in the non-linear advection terms and a biharmonic diffu-
 104 sion operator to improve the PV dynamics ([Winther et al., 2007, Morel and McWilliams, 2001,
 105 Herbette et al., 2003]). This model solves the shallow water equations which, for the two-layer
 106 configurations considered here, can be expressed as :

$$\partial_t \mathbf{u}_k + (\mathbf{u}_k \cdot \nabla) \mathbf{u}_k + f_0 \mathbf{k} \times \mathbf{u}_k = -\nabla \mathcal{M}_k + F_k + T_k^w, \quad (1)$$

$$\partial_t h_k + \nabla \cdot (\mathbf{u}_k h_k) = 0, \quad (2)$$

107 where k is the layer number (here, $k = 1$ for the top layer and $k = 2$ for the bottom one),
 108 $\mathbf{u}_k = (u_k, v_k)$ is the horizontal velocity, $f_0 = 10^{-4} s^{-1}$ is the Coriolis parameter (considered
 109 constant here), h_k is the thickness of the isopycnal layer k , T_k^w represents the wind forcing, and
 110 F_k contains the frictional and viscosity terms (horizontal diffusion is associated with a bihar-
 111 monic operator with a viscosity that depends on the velocity modulus and deformation tensor,

112 see [Winther et al., 2007]). Finally, \mathcal{M}_k is the Montgomery potential (pressure along an isopyc-
 113 nal surface), which can be written :

$$\mathcal{M}_k = \sum_{i=1}^2 g h_i + \sum_{i=1}^{k-1} \frac{\rho_i - \rho_k}{\rho_k} g h_i, \quad (3)$$

114 where ρ_i is the density of the isopycnic layer i and g is the gravity acceleration.

115 2.2. Configuration and parameters

116 The configuration is a periodic zonal channel on an f -plane, with vertical side walls on the
 117 northern and southern boundaries. The bottom is flat except near the southern boundaries in the
 118 middle of the domain where there exists a promontory. As shown in figure 2, the promontory is
 119 composed of a flat plateau of variable height H_t , length L_y and width L_x , rounded at its offshore
 120 edge, and surrounded by a Gaussian slope of a variable extension dL (figure 2). To represent a
 121 mid latitude summer thermocline, the surface layer depth at rest $H_1 = 50$ m and the bottom layer
 122 depth away from the promontory is $H_2^\infty = 2000$ m for most experiments. The upper layer density
 123 is fixed to $\rho_1 = 1000 \text{ kg/m}^3$, the water column stratification is defined by the reduced gravity
 124 $g' = g(\rho_2 - \rho_1)/\rho_1$. Unless stated otherwise (when testing the sensitivity to the stratification
 125 characteristics) $g' \simeq 0.01$.

126 $R_d = \sqrt{g' H_1 H_2 / (H_1 + H_2)} / f_0$ is the Rossby radius of deformation, and $R_d \simeq 7 \text{ km}$ ($H_1 =$
 127 50 m, $H_2^\infty = 2000$ m, $f_0 = 10^{-4} \text{ s}^{-1}$ and $g' = 1^\circ/oo$) for most of the experiments presented
 128 below. !!!!!YM This value is smaller than the usual Rossby radius of deformation observed
 129 in the deep ocean (around 20 km). It is however consistent with the upper ocean stratification
 130 in summer (when the seasonal pycnocline has been formed) and corresponds to mid-slope or
 131 shelf characteristics. In addition, sensitivity experiments where the Rossby Radius is varied will
 132 show that this parameter has a weak influence on the processes studied here (see section 4.2).
 133 !!!!!YM

134 The parameters corresponding to the various simulations presented below can be found in
 135 table 1 (fixed parameters) and 2 (variable parameters).

136 2.3. Potential vorticity and potential vorticity anomaly

137 For the shallow water model used here, the potential vorticity for each isopycnic layer is
 138 defined as :

$$PV_k = \frac{f_0 + \zeta_k}{h_k}, \quad (4)$$

139 where $\zeta_k = \nabla \times \mathbf{u}_k = \partial_x v_k - \partial_y u_k$ is relative vorticity in layer k , and h_k is the layer thick-
 140 ness. In the absence of diabatic process, PV is conserved for each fluid particle. PV is
 141 also related to the velocity field that can then be calculated by inverting the PV field un-
 142 der the assumption of (cyclo-)geostrophic equilibrium. PV conservation and invertibility
 143 are key properties which helped understand and interpret many geophysical fluid processes
 144 ([McWilliams and Gent, 1980], [McIntyre and Norton, 1990], [Hoskins et al., 1985], see also
 145 [Morel et al., 2006, Rossi et al., 2009] for applications to upwelling dynamics).

146 PV is finite at rest and in order to invert it and to calculate the velocity, we use the potential
 147 vorticity anomaly (PVA) which is defined in each layer k as the difference between the local PV

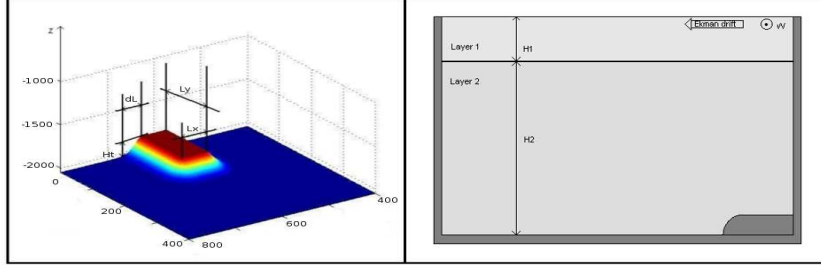


Figure 2: a : Details of the promontory : It is centered on $x = 300\text{km}$. L_x and L_y are respectively the length and width of its flat top, H_t its height, and dL is the typical length of its Gaussian sloping sides. b : Model configuration at rest : a shallow surface layer of depth H_1 and density ρ_1 lies over a bottom layer of depth H_2 and density ρ_2 . The numerical domain is a periodic zonal channel with vertical walls and a flat bottom.

148 and a reference PV for a state at rest (no current and flat isopycnals) (see [*Herbette et al.*, 2003,
149 *Herbette et al.*, 2005, *Rossi et al.*, 2009]) :

$$PVA_k = H_k (PV_k - PV_k^{ref}) = H_k \left(\frac{f_0 + \zeta_k}{h_k} - \frac{f_0}{H_k} \right) = \frac{H_k}{h_k} (\zeta_k - f_0 \frac{\delta h_k}{H_k}), \quad (5)$$

150 where $H_k(x, y)$ is the layer thickness at rest, and $\delta h_k = h_k - H_k$. Notice that we have also multiplied
151 the PV difference by the layer thickness at rest so that PVA is proportional to the vorticity, which
152 makes it easier to analyze. PVA contains the dynamical signal associated with the PV field and
153 the geostrophic velocity field can be inferred from the PVA field. Notice that, as H_k is a function
154 of position, contrary to PV , PVA is not conserved for each particle in the presence of a variable
155 bottom topography. It is however directly related to the circulation. The presence of a PVA pole
156 in a layer k is indeed associated with a circulation extending to all layers but intensified in layer k
157 ([*Hoskins et al.*, 1985, *Rossi et al.*, 2009]) : a positive PVA pole being associated with a cyclonic
158 circulation, a negative one with an anticyclonic circulation.

159 As shown in [*Verron and Le Provost*, 1985, *Herbette et al.*, 2003], when a current develops
160 above a seamount, two opposite sign eddies appear : an anticyclone trapped above the topo-
161 graphic feature associated with the displacement of low PV water columns from the deep ocean
162 upon the seamount and a cyclone associated with the advection of high PV water columns off
163 the topography. Figure 3) describes this process which is adiabatic and relies on the advection
164 of PV and the formation of PVA poles. It also shows that between the two opposite sign eddies
165 a strong jetlike current is formed.

166 2.4. Previous results and general upwelling characteristics

167 [*Morel et al.*, 2006] found an exact analytical solution for the geostrophic circulation of a 2-D
168 configuration with a flat bottom and a constant wind forcing T^w . In practice, $T^w = \tau^w / (\rho_1 h_1)$

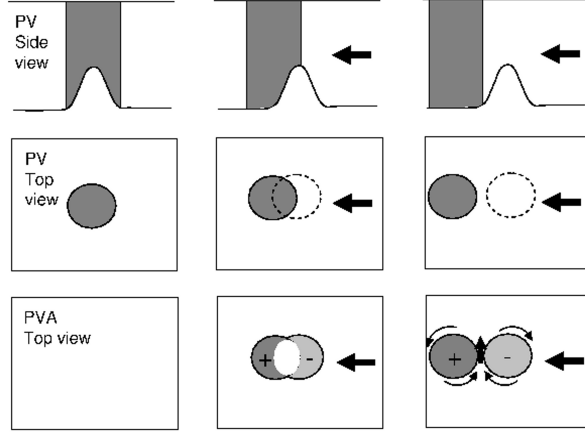


Figure 3: Schematic view of the development of a topographic dipole when a current develops above a seamount. The initial PV structure (top panels for the side view and middle panels for the top view) is associated with high PV above the seamount and lower PV in the deeper ocean; the fluid is initially at rest and the PVA (lower panels) is null. The current exchanges the position of low and high PV water columns which forms positive and negative PVA. An anticyclonic circulation develops above the topography whereas a cyclonic circulation is associated with the high PV water columns detaching from the seamount. The current is intensified between the opposite sign eddies.

169 (where τ^w is the surface wind stress) is not constant but, with the approximation $T^w = \tau^w / (\rho_1 H_1)$,
 170 the following formulas provide a good evaluation for the position of the outcropping front and
 171 velocity field as a function of the wind stress intensity and the duration of the wind forcing. It is
 172 then possible to obtain a stationary basic state current with the desired characteristics by limiting
 173 the forcing to a chosen period for a given wind stress intensity.

174 The distance of the outcropping front from the coast is :

$$Y(t) = \min\{0, -\frac{T^w}{f(1 + \delta)}(t - t_0)\} \quad (6)$$

$$t_0 = \frac{fR_d(1 + \delta)}{T^w} \quad (7)$$

175 and the alongshore velocity field in both layers is given by :

176 if $y < Y(t)$

$$U_1 = U_c \exp \frac{y}{R_d} + U_b(t), \quad (8)$$

$$U_2 = -\delta U_c(t) \exp \frac{y}{R_d} + U_b(t), \quad (9)$$

177 if $y \geq Y(t)$

$$U_1 \quad \text{undefined}, \quad (10)$$

$$U_2 = -f\delta(y - Y(t)) - \delta U_c(t) \exp \frac{Y}{R_d} + U_b(t). \quad (11)$$

178 where $\delta = H_1/H_2$, t_0 is the time necessary for the lower layer to outcrop at the coast ($y = 0$). $U_b(t)$

179 and $U_c(t)$ are the temporal evolution of the barotropic and baroclinic components respectively
 180 and can be written as :
 181 if $t < t_0$

$$U_b = \frac{\delta T^w}{1 + \delta} t \quad (12)$$

$$U_c = \frac{T^w}{1 + \delta} t \quad (13)$$

182 if $t \geq t_0$

$$U_b = \frac{\delta T^w}{1 + \delta} t \quad (14)$$

$$U_c = f R_d \exp \frac{-Y(t)}{R_d} \quad (15)$$

183 Notice that the maximum current is reached at the outcropping front (for $t \geq t_0$) and is given
 184 by:

$$\begin{aligned} U_1^{max} &= f R_d + \frac{\delta T^w}{1 + \delta} t \\ &= (1 + \delta) f R_d + \delta f |Y(t)| \end{aligned} \quad (16)$$

185 Notice that the barotropic mode is spatially constant and only the cross shore spatial structure
 186 of the baroclinic mode varies as $\exp \frac{y}{R_d}$. In addition, the amplitude of the baroclinic component
 187 of the velocity field is limited whereas the barotropic one grows linearly with time (until other
 188 processes such as bottom friction become non-negligible).

189 The wind stress corresponding to a 30 knots wind (15 m/s) is $\tau^w \simeq 0.2 N/m^2$ and thus we get
 190 $T^w \simeq 4 \cdot 10^{-6} m/s^2$ (for $H_1 = 50 m$). Then, the previous formulas show that it takes about
 191 $t_o \simeq 2$ days for the outcropping front to be generated and after 10 days of wind forcing, the front
 192 is located $Y \simeq 35 km$ offshore and the maximum velocity at the front is about $U_1^{max} \simeq 70 cm/s$.
 193 The barotropic velocity, and the velocity field in the deep layer over most of the domain, are
 194 $U_b \simeq 8 cm/s$. The characteristics of the upwelling found in the numerical simulations presented
 195 below are in very good agreement with these analytical results.

196 3. Reference experiment

197 The wind forcing was kept constant $T^w = \tau^w / (\rho_1 H_1)$ in the reference simulation that we
 198 present here.

199 Figure 4 shows the evolution of the *PVA* in the upper layer superimposed on the shape of the
 200 promontory for the reference experiment (see table 2). During the upwelling development, the
 201 upper layer vanishes close to the coast and is replaced by deep waters that reach the sea surface.
 202 This area is associated with an infinite *PVA* in the upper layer (see [Bretherton, 1966]) and is thus
 203 delimited by a strong *PVA* gradient that we use to trace the upwelling front and the development
 204 of the upwelling filaments (it is qualitatively comparable to the sea surface temperature front).

205 The strong *PVA* gradient associated with the upwelling front becomes evident on the third
 206 day of the experiment. It is accompanied by an intense baroclinic surface intensified jet super-
 207 imposed on a spatially constant barotropic westward flow. The influence of bottom topography

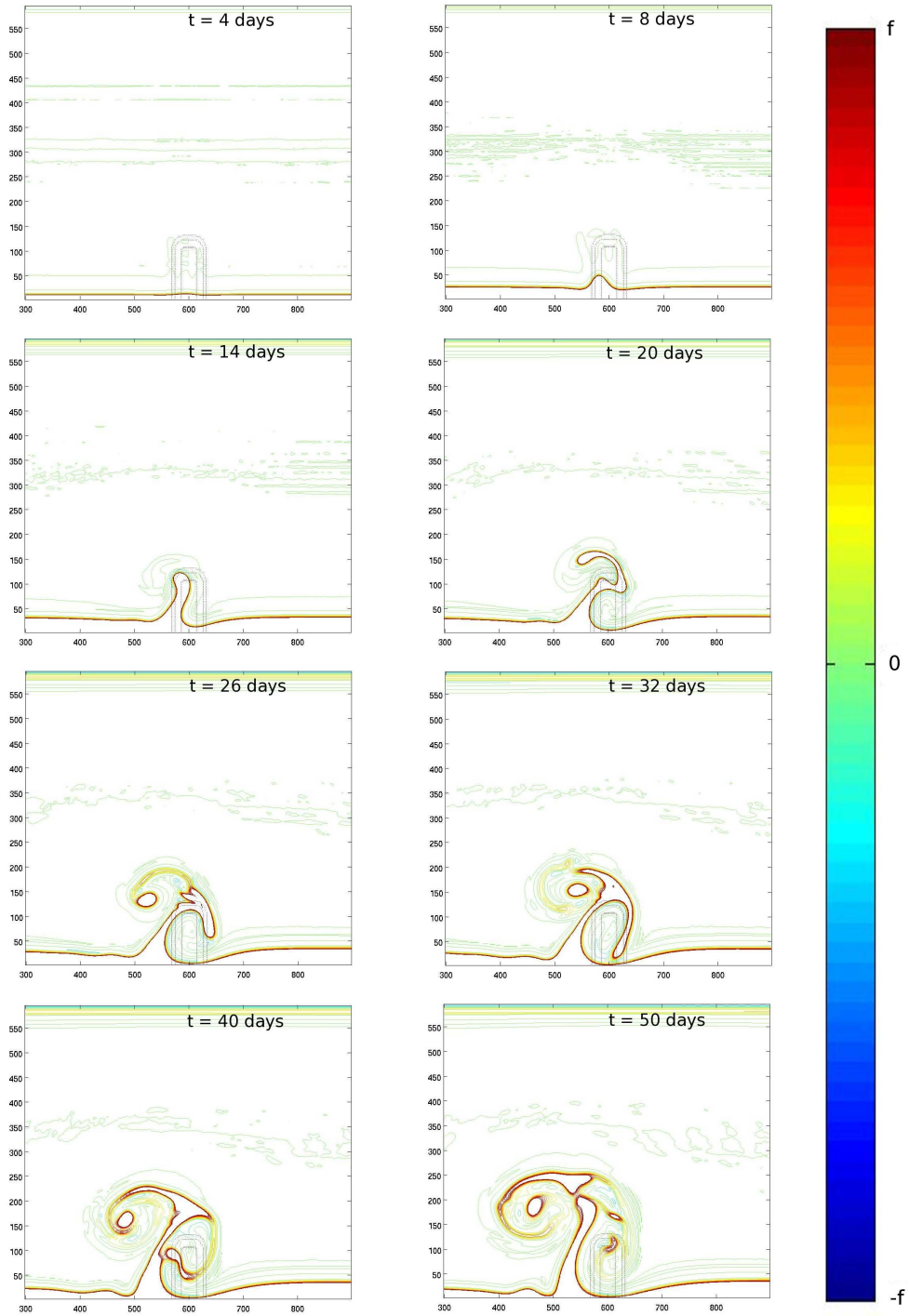


Figure 4: Evolution of the PVA in the upper layer for the reference experiment at $t = 4, 8, 14, 20, 26, 32, 40, 50$ days. The thick red line represents the $PVA = +f$ contour and is a good marker of the upwelling front. The axis are labelled in km.

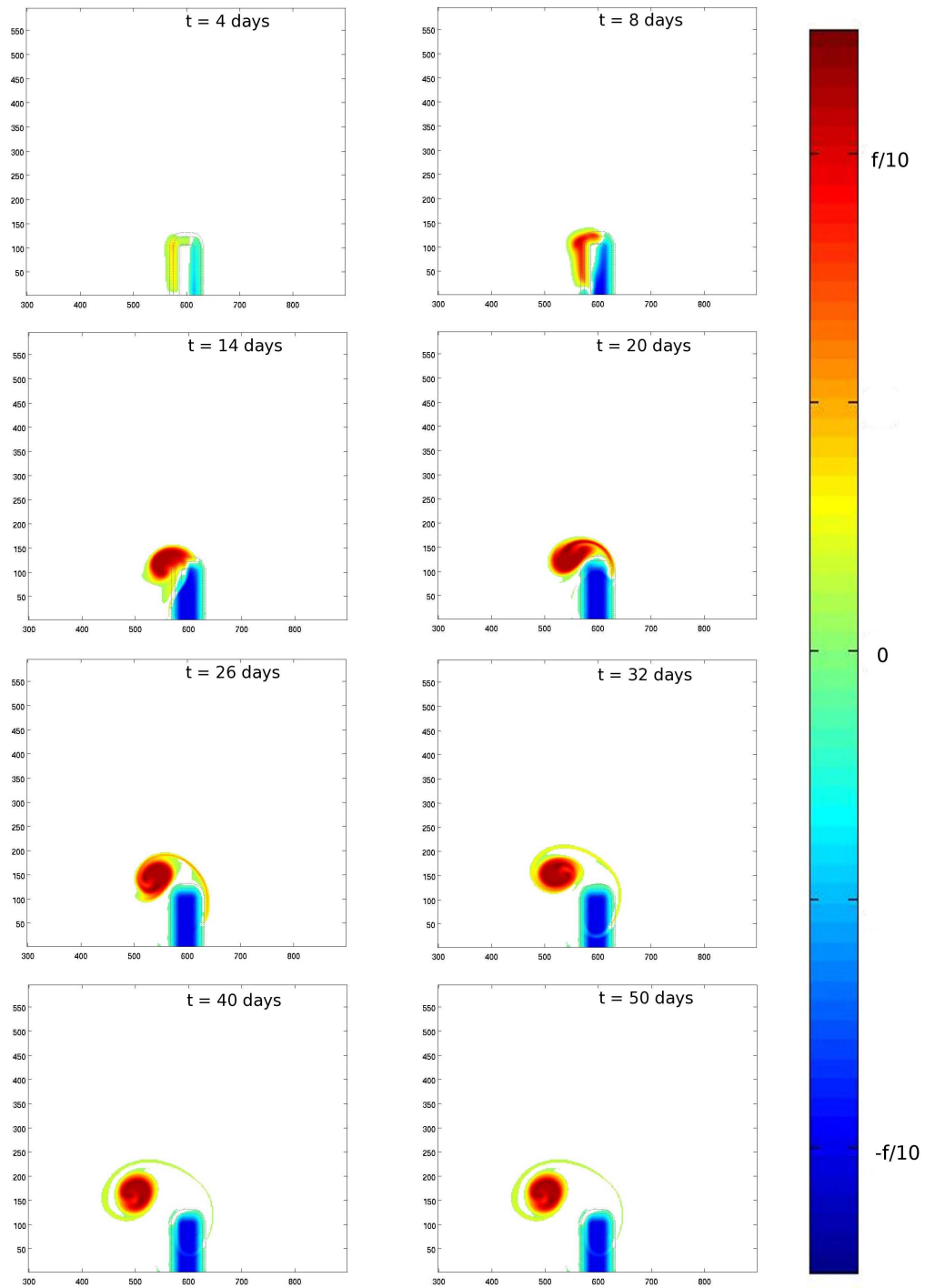


Figure 5: Evolution of the PVA in the bottom layer for the reference experiment at $t = 4, 8, 14, 20, 26, 32, 40, 50$ days. The generation of PVA is visible in the first 10 days. It is then advected from day 10 to day 50.

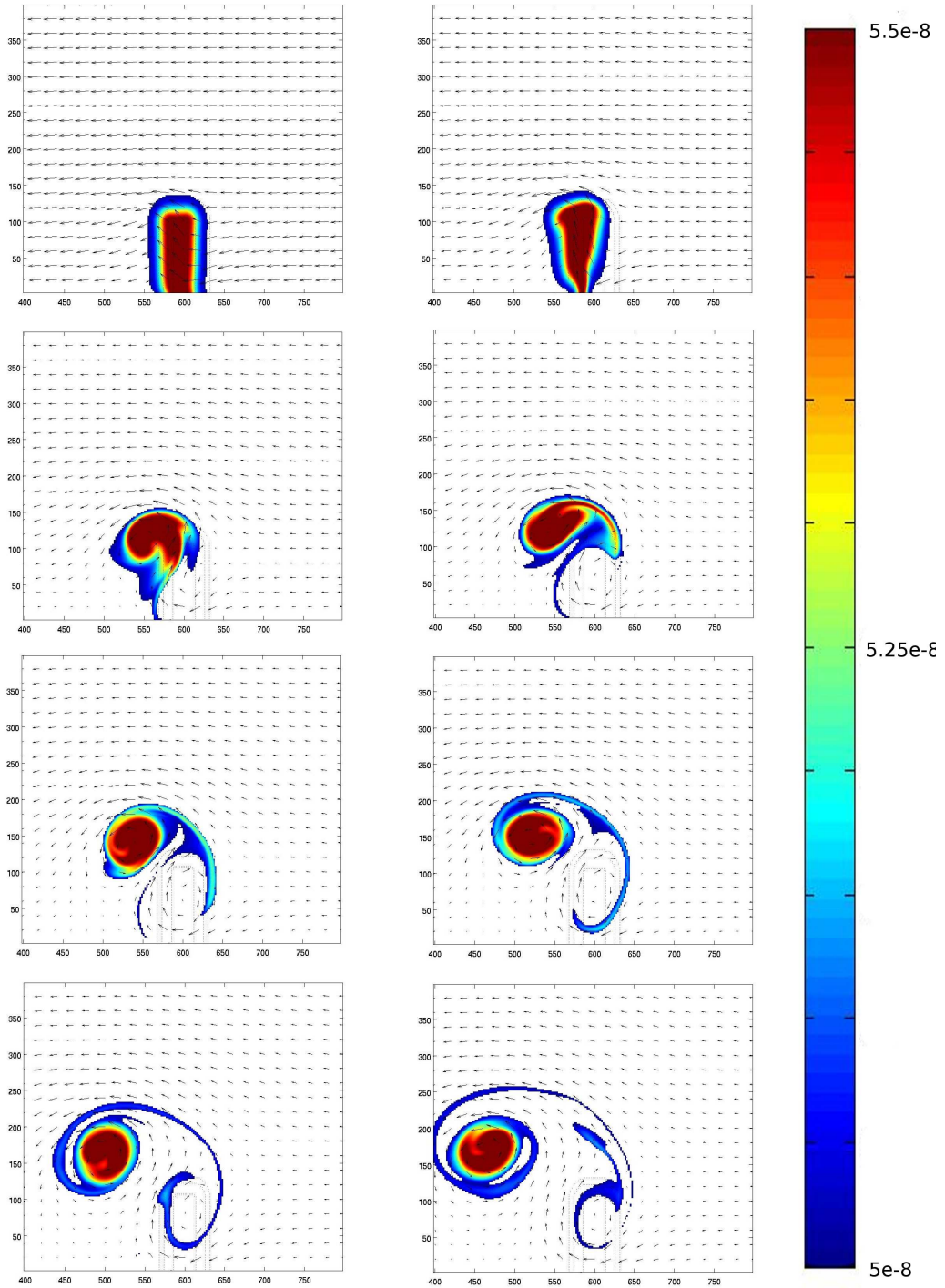


Figure 6: Evolution of the bottom layer absolute potential vorticity for the reference experiment superimposed on the velocity field. The high PV pool is visible on the promontory. Note that potential vorticity is strictly conserved and is only advected by the current. Comparison with Fig. 5 also shows that the anticyclonic and cyclonic circulations are associated with the negative and positive PVA poles that develop because of bottom topography, as expected.

208 is noticeable after 4 days, when the front begins to form a small meander on the western (down-
 209 stream) side of the promontory. The initial topographical meander keeps on growing offshore
 210 downstream of the promontory. After 12 days of simulation, it starts to roll up anticyclonically
 211 around the promontory. At day 16, another branch appears, growing offshore but partly rolling
 212 up cyclonically. The meander has then become a thin and elongated filament, surrounded by
 213 two counter-rotating recirculations. Its length is about 200 km and its width about 100 km near
 214 the coast and 20 km near the tip. It is similar to the 'squirts', observed in all major upwelling
 215 systems. After 28 days, the filament is still growing offshore and is about 220 km long, but its
 216 offshore edge has rolled up cyclonically. As shown on Fig. 4, the filament continues to grow
 217 until the end of the simulation (it is about 230 km long after 50 days), corresponding to a mean
 218 growth rate of about 5 km per day for the whole life cycle, consistent with the observed mean
 219 value found by [Kostianoy and Zatsepin, 1996]. But the growth rate of the filament is variable
 220 during the life cycle, with higher initial growth rates of up to 12 km day^{-1} (i.e. 14 cm s^{-1}) after
 221 10 days, then decreasing until the end of the experiment.

222 The formation of the filament is very similar to the erosion process of a surface vortex by
 223 a seamount studied in [Herbette et al., 2003]. As already explained above, the origin of these
 224 counter-rotating eddies can indeed be inferred from the PV and PVA evolution in the lower
 225 layer. Indeed, as shown in [Morel et al., 2006, Rossi et al., 2009] a barotropic westward current
 226 is generated during the upwelling development. The baroclinic circulation opposes this current
 227 in the upper layer, but its extension is of the order of the first internal radius of deformation
 228 (about 7km here) which is quite small. As a result, water columns move westward over most of
 229 the lower layer. As the dynamics is adiabatic here, the initial PV field is simply advected and
 230 the positive anomaly associated with the promontory moves downstream (see Fig. 6) replaced
 231 by lower PV water columns coming from deeper region. Figure 5 shows that it creates opposite
 232 sign PVA (see also [Herbette et al., 2003]): high PV water columns coming from the promontory
 233 move in regions with lower PV at rest, forming a positive PVA downstream of the promontory,
 234 while low PV water columns move upon the promontory, which is associated with high PV at
 235 rest, forming a negative PVA that is being trapped above the promontory. As shown in Fig. 6,
 236 this topographic PVA dipole is associated with cyclonic and anticyclonic circulations extending
 237 over the whole water column. An offshore jetlike current develops between the two opposite sign
 238 PVA poles, which forms the filament.

239 After 7 days both positive and negative PVA reach a maximum modulus of $\pm 0.1f$, the nega-
 240 tive PVA obviously remains trapped above the topography, maintaining offshore currents on the
 241 western side of the promontory which reach about 40 cms^{-1} . But the high PVA pole is strongly
 242 deformed and propagates offshore and westward under the combined effect of advection and in-
 243 teraction with bottom topography. The topographic β -drift of a PVA pole along the slope of the
 244 promontory scales -in the quasi-geostrophic approximation- as $U_{drift} = \beta_t R_d^2$, with $\beta_t = f_0 \alpha / H_2$
 245 where $\alpha = H_t / dL$ is the characteristic slope of the promontory, and R_d^2 is the square of the Rossby
 246 radius. For the reference experiment, U_{drift} is found to be about 2.5 cms^{-1} . The barotropic ve-
 247 locity field associated with a PVA pole in the lower layer can be scaled using the circulation
 248 theorem :

$$U^- \approx C / 2\pi l \quad (17)$$

$$C = \int \int_P PVA \frac{h_2}{H_{tot}} dS \quad (18)$$

$$\simeq \int \int_P PVA \, dS \quad (19)$$

249 where C is the circulation or total PVA reservoir inside a domain P , l is the distance from the
 250 center of the PVA pole, $H_{tot} = H_1 + H_2$ and dS is the surface element. If we assume that all water
 251 columns above the promontory have been replaced by water columns coming from the deeper
 252 ocean, the negative PVA forming above the promontory is given by :

$$PVA = -\frac{f H_p(x, y)}{H_2^\infty} \quad (20)$$

253 where $H_p(x, y)$ is the the promontory height.

254 The total circulation associated with the negative PVA of the promontory, over the domain P
 255 is then

$$C = -\frac{f}{H_2} \int \int_P H_p(x, y) dS \quad (21)$$

$$\simeq -\frac{f}{H_2} H_t [L_x L_y + dL (L_x + L_y/2)] \quad (22)$$

256 For the positive pole, the calculations are similar : the PVA reservoir, and thus circulation, is
 257 exactly the opposite of the negative one above the promontory (water columns are exchanged
 258 between the deep ocean and the promontory). As the effect of both PVA poles superimposes, the
 259 maximum barotropic current between both poles is thus roughly given by :

$$U_{max}^{jet} \simeq 2C/2\pi l \quad (23)$$

$$C \simeq \frac{f}{H_2} H_t [L_x L_y + dL (L_x + L_y/2)] \quad (24)$$

260 where l is the mid distance between both pole centers.

261 When both PVA poles are well developed, $l \simeq 30$ km and $U_{max}^{jet} \simeq 36$ cm/s, which is the
 262 order of magnitude of the maximum offshore current observed downstream of the promontory
 263 (40 cm/s). These modelled velocities are in very good agreement with what have been observed
 264 in-situ in the IPUS area and also in other upwelling regions (see [Sanchez *et al.*, 2008]).

265 Notice that the estimation of U_{max}^{jet} or U^- is only correct in the case of circular PVA structures,
 266 or far enough from the structure so that shape effects become negligible. Here, this is obviously
 267 not verified, but, using this simple scaling can give us a good insight of the order of magnitude
 268 of the velocity associated with the topographic PVA pole development and its sensitivity to the
 269 promontory characteristics.

270 In summary, an anticyclonic circulation is generated and trapped above the promontory by
 271 advection of low PV over the topography, forming a negative PVA pole. A cyclonic circulation
 272 also forms because of advection of high PV from the promontory into a deeper environment.
 273 This forms a trapped topographic dipole associated with a strong offshore current that generates
 274 the filament and its well known 'squirt' or 'mushroom' shapes (see [Strub *et al.*, 1991]). The
 275 strength of the current depends on the total PVA reservoir of the promontory.

276 Finally, notice that, even though the initial topographic cyclone slowly separates from the
 277 trapped anticyclone, because of the outcropping and vanishing of the upper layer, the meander
 278 and filament are themselves also associated with an equivalent high PVA (see [Bretherton, 1966])
 279 reinforcing and maintaining a cyclonic circulation on the downstream side of the negative PVA
 280 pole.

281 4. Sensitivity experiments

282 To strengthen the physical relevance of the mechanism described above and to assess the
283 respective importance of the various parameters and characteristics of the configuration, a set of
284 sensitivity tests was performed. Here we focused on the stability of the front, the forcing duration
285 time, of the promontory characteristics (width, length, height and slopes), of the stratification and
286 of bottom friction. For comparison of the various model output, we take as a reference time the
287 $t = 42$ days (6 weeks) output, and use the *PVA* maps as a qualitative indicator of the efficiency
288 of the model configuration to produce long, coherent and trapped filaments.

289 4.1. The stability of the front

290 The reference run showed that the sole presence of the topography allowed the de-
291 velopment of a long filamentary structure reaching as far as 230 km offshore. How-
292 ever, mixed barotropic-baroclinic instability is a well known feature of upwelling currents
293 [*Shi and Roed, 1999*] and has sometimes also been referred to as the main process for filament
294 formation [*Haidvogel et al., 1991*]. It is thus important to evaluate the relative influence of to-
295 pography and intrinsic instability on the development of the long filament.

296 Baroclinic instability can only develop when there exists opposite sign potential vorticity gra-
297 dients or *PVA* (see [*Charney and Stern, 1962*]). The outcropping front is associated with positive
298 *PVA*. As shown by [*Morel et al., 2006*], negative *PVA* is generated along the upwelling front
299 (see Fig. 7 below) because as isopycnic surfaces bend upward they enter the region influenced
300 by the wind stress. A wind stress curl then exists along isopycnic levels which has been shown to
301 necessarily form negative *PVA* (the formation of negative *PVA* by the wind has also been studied
302 in [*Thomas, 2005*]). In the simple 2-layer configuration used here, this effect is associated with
303 the fact that $T^w = \tau^w / (\rho_1 h_1)$ varies with the layer depth h_1 .

304 In the reference experiment, the possibility of the flow to become baroclinically unstable has
305 thus been suppressed by modifying the distribution of the wind forcing : $T^w = \tau^w / (\rho_1 H_1)$ pro-
306 vides a constant wind stress so that the upwelling still develops but the dynamics remains adia-
307 batic and the PV field is conserved. As a result, no negative *PVA* is formed along the front and
308 no baroclinic instability can develop.

309 In the present test, we use the actual wind forcing $T^w = \tau^w / (\rho_1 h_1)$. Figures 7 and 8 show
310 the evolution of the *PVA* in the upper layer and in the lower layer respectively. In compari-
311 son with the reference experiment (see Fig. 4 and 5), negative *PVA* is develops along the up-
312 welling front. This negative *PVA* strip interacts with the positive *PVA* associated with the out-
313 cropping forming new small-scale meanders, with wavelengths of 30 km after 10 days (notice
314 the association of the small upwelling front meanders with small negative *PVA* poles). These
315 small-scale meanders are associated with baroclinic (or sometimes called frontal) instabilities
316 ([*Barth, 1989 a, Barth, 1989 b, Morel et al., 2006, Capet and Carton, 2004, Killworth, 1980*])
317 but are neither trapped nor forming long filaments. They indeed propagate along the upwelling
318 front, re-enter the domain on the eastern side and only very slowly develop after their initial
319 growing. After 5 weeks of experiment, their offshore extension is less than 50 km (from the
320 front).

321 The impact on the main filament is also minor: the positive and negative *PVA* poles still
322 develop in the bottom layer and their time evolution is not significantly modified. The surface
323 filament is very similar to the one observed in the stable case and it extends as far offshore. The
324 only noticeable difference, apart from the absence of the small amplitude meanders along the
325 front, is that the topographic filament is here truncated by the small scale eddies and also appears

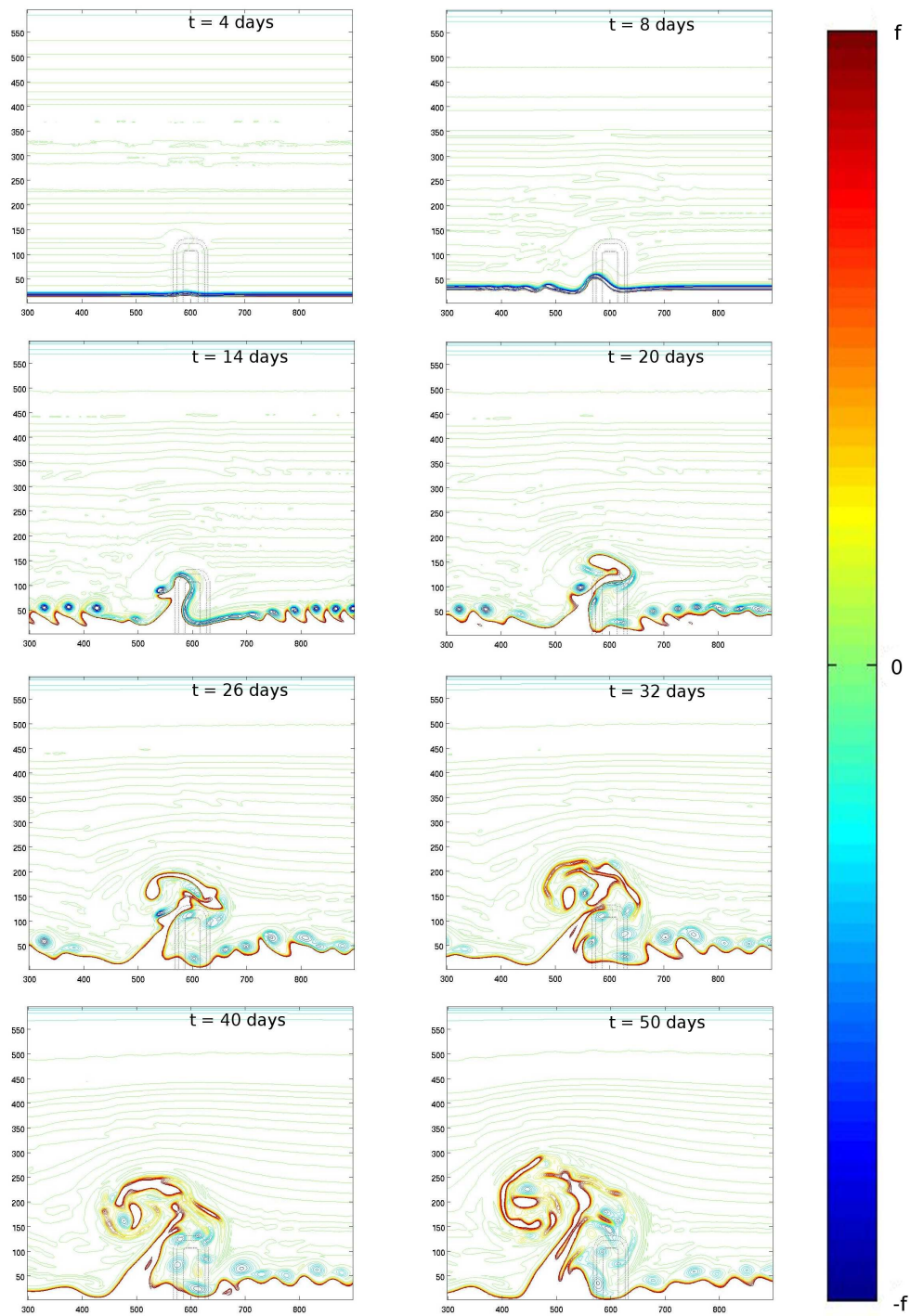


Figure 7: Evolution of the PVA in the upper layer for the unstable experiment at $t = 4, 8, 14, 20, 26, 32, 40, 50$ days. Notice the additional smaller meanders, but the formation of the large filament is the same as in Fig. 4.

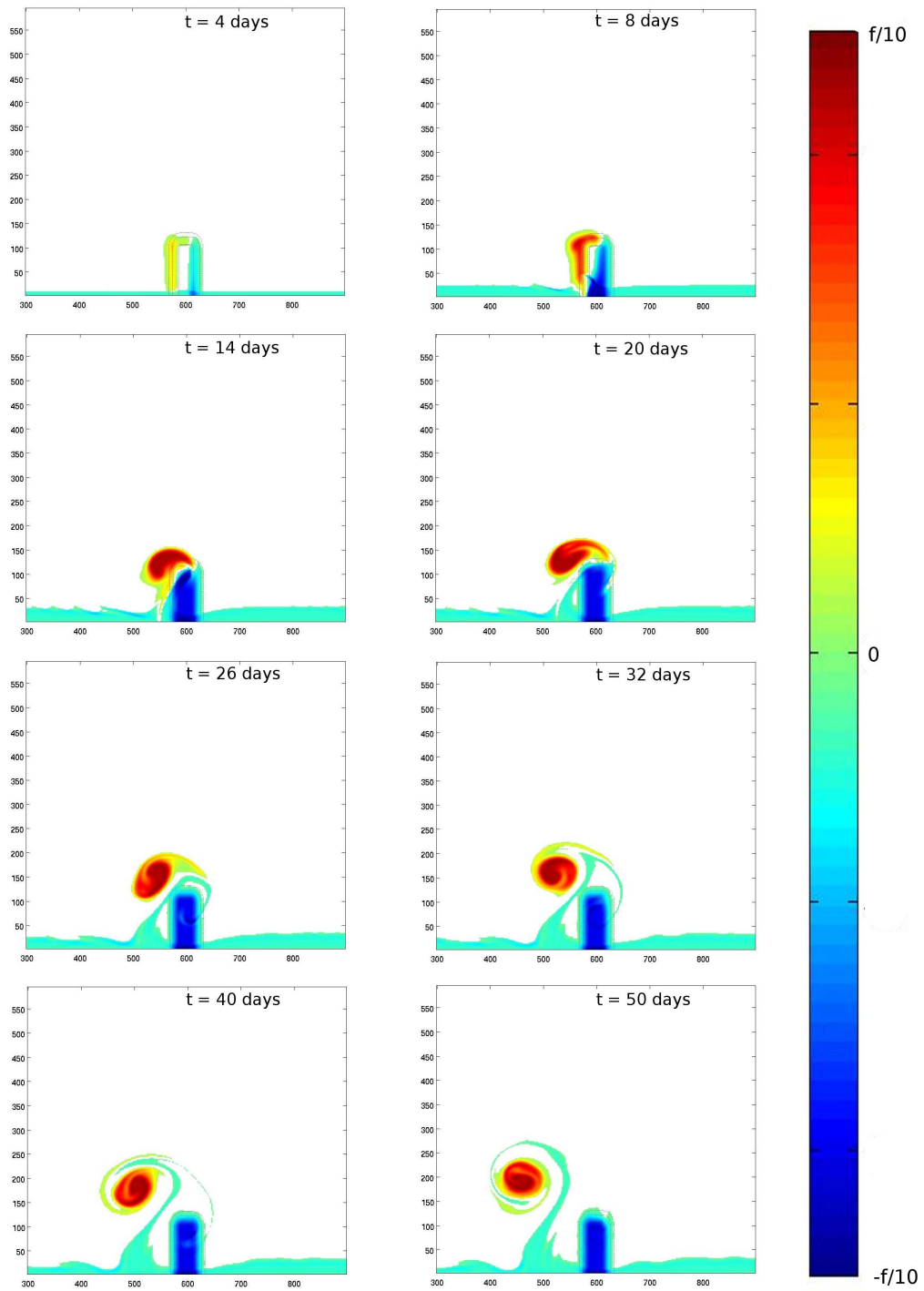


Figure 8: Evolution of the PVA in the bottom layer for the unstable experiment at $t = 4, 8, 14, 20, 26, 32, 40, 50$ days.

326 slightly larger at its base. This proves that, at least in our simplified configuration, intrinsic
327 baroclinic instability has little influence on the formation of the long filament and that the main
328 mechanism is associated with topography, as described above.

329 The stable front configuration is also of particular interest because the dynamics is adiabatic
330 and PV is conserved following fluid parcels in all layers and can be used as a tracer. For this
331 reason, and because we have shown that no substantial difference existed in the formation of the
332 filament, we keep the stable front configuration as our reference experiment for the following
333 sensitivity tests that will thus be carried with the modified and constant wind forcing.

334 4.2. The influence of the stratification characteristics

335 In addition to the reference experiment ($g' = 0.01$, $H_1 = 50$ m), six additional experiments were
336 performed to evaluate the influence of the stratification characteristics on the dynamics of the
337 topographic filament : 3 experiments varying g' (0.005, 0.02 and 0.03 ms^{-2}), and 3 experiments
338 varying H_1 (25, 100, and 200 m). It may seem redundant to vary both parameters (as they
339 both influence the Rossby radius) but we finally found out that their respective influence on the
340 upwelling front evolution is quite different.

341 Figure 9 represent the upper layer PVA after 42 days for different values of g' and shows
342 only modest modification of the filament. This is not entirely surprising as the density jump
343 mostly influences the baroclinic currents in the vicinity of the front via the Rossby radius of
344 deformation. Topographic eddies are formed and influence the dynamics through the barotropic
345 circulation, which is not modified. In addition, the position of the upwelling front is also only
346 slightly affected by a modification of g' : the offshore displacement is not modified and only the
347 initial time at which the outcropping front forms depends on this parameter.

348 Varying H_1 (Fig. 10) does not modify the lower layer dynamics either (see the similarities
349 of the PVA structure in the lower layer after 42 days on the right panels of Fig. 10). However,
350 since it also plays a role in the strength of the wind forcing ($T^w = \tau^w / (\rho_1 H_1)$), it strongly mod-
351 ifies the position of the upwelling front, which forms later and extends more slowly for deeper
352 thermoclines (larger H_1). The differences in the filament evolution with different H_1 is thus the
353 result of the time lag between the upwelling front evolution associated with H_1 and the distribu-
354 tion of the topographic eddies when the outcropping first forms. As a result, the advective effect
355 of the topographic eddies on the upwelling front is in general simply delayed. The time period
356 necessary for the upwelling front to be formed is $t_o \approx 0.7, 2, 6$ and 16 days for $H_1 = 25, 50,$
357 100 and 200 m respectively. As a result, for the duration of the wind forcing considered here
358 (10 days), varying H_1 does not strongly modify the filament except for the deepest thermocline
359 (here associated with the case $H_1 = 200\text{m}$) for which the upwelling front is not formed and no
360 filament is then visible (see Fig. 10 lower panel). Interestingly, the final offshore extent has close
361 values for the all other experiments.

362 Finally notice that the experiment where g' is varied and the experiment where H_1 is varied
363 have different Rossby radius of deformation : $R_d = 5, 7, 10, 14$ km, for $H_1 = 25, 50, 100, 200$
364 m respectively (or $g' = 0.005, 0.01, 0.02$ and 0.03 respectively). This underlines again that
365 the important mechanisms for the filament development is the barotropic circulation and the
366 formation of the upwelling front. In our configuration the development of the filament is mainly
367 controlled by the bottom layer PVA evolution which is almost insensitive to R_d .

368 4.3. The forcing duration time

369 We here study the effect of a variation of the wind forcing duration time. As seen above, the
370 wind forcing acts both on the offshore front position and the velocity strength, especially the one

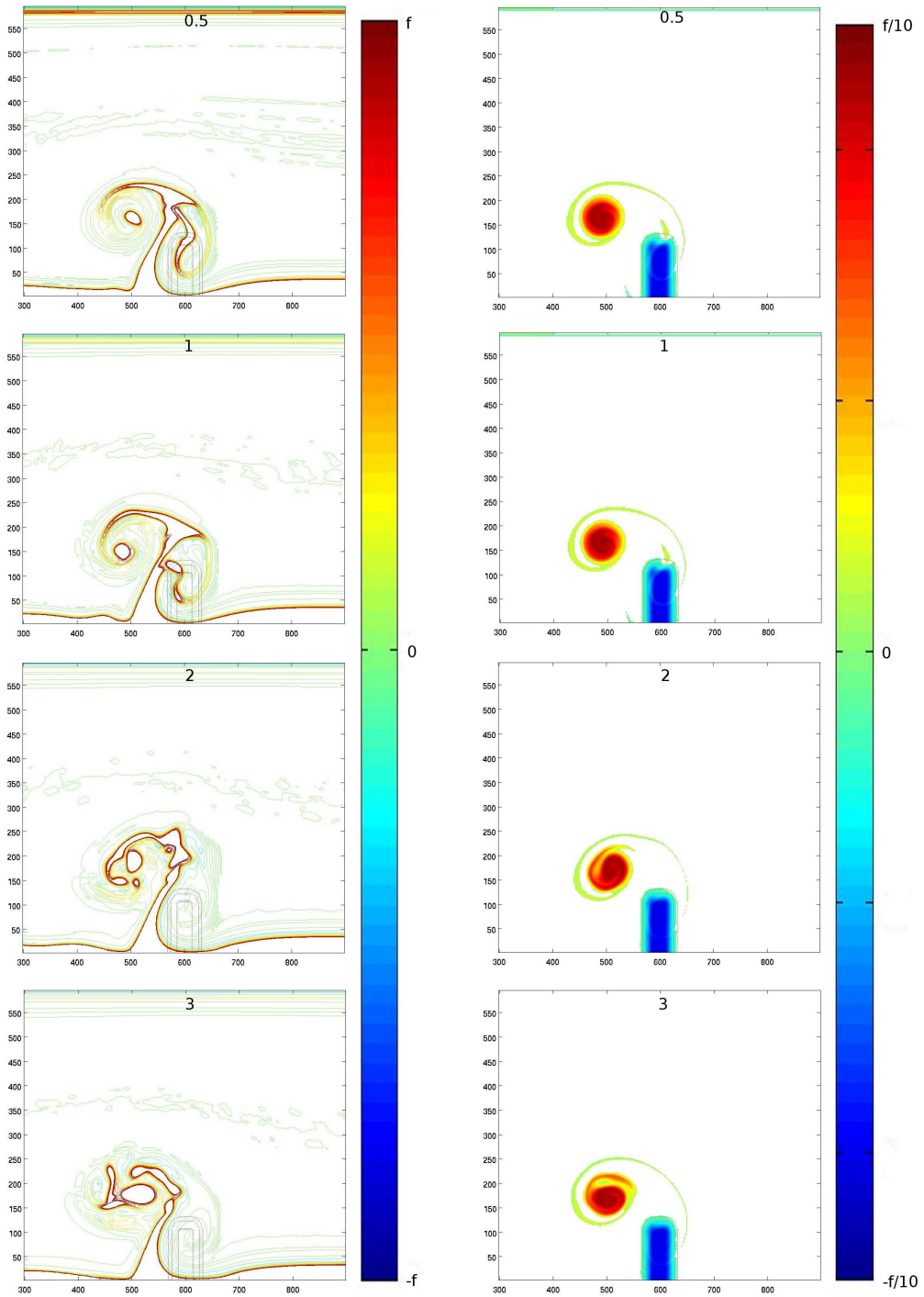


Figure 9: Maps of *PVA* in the upper (left hand panel) and bottom (right hand panel) layers at $t = 42$ days for the $g' = 0.005, 0.01, 0.02$ and 0.03ms^{-2} experiments. !!!

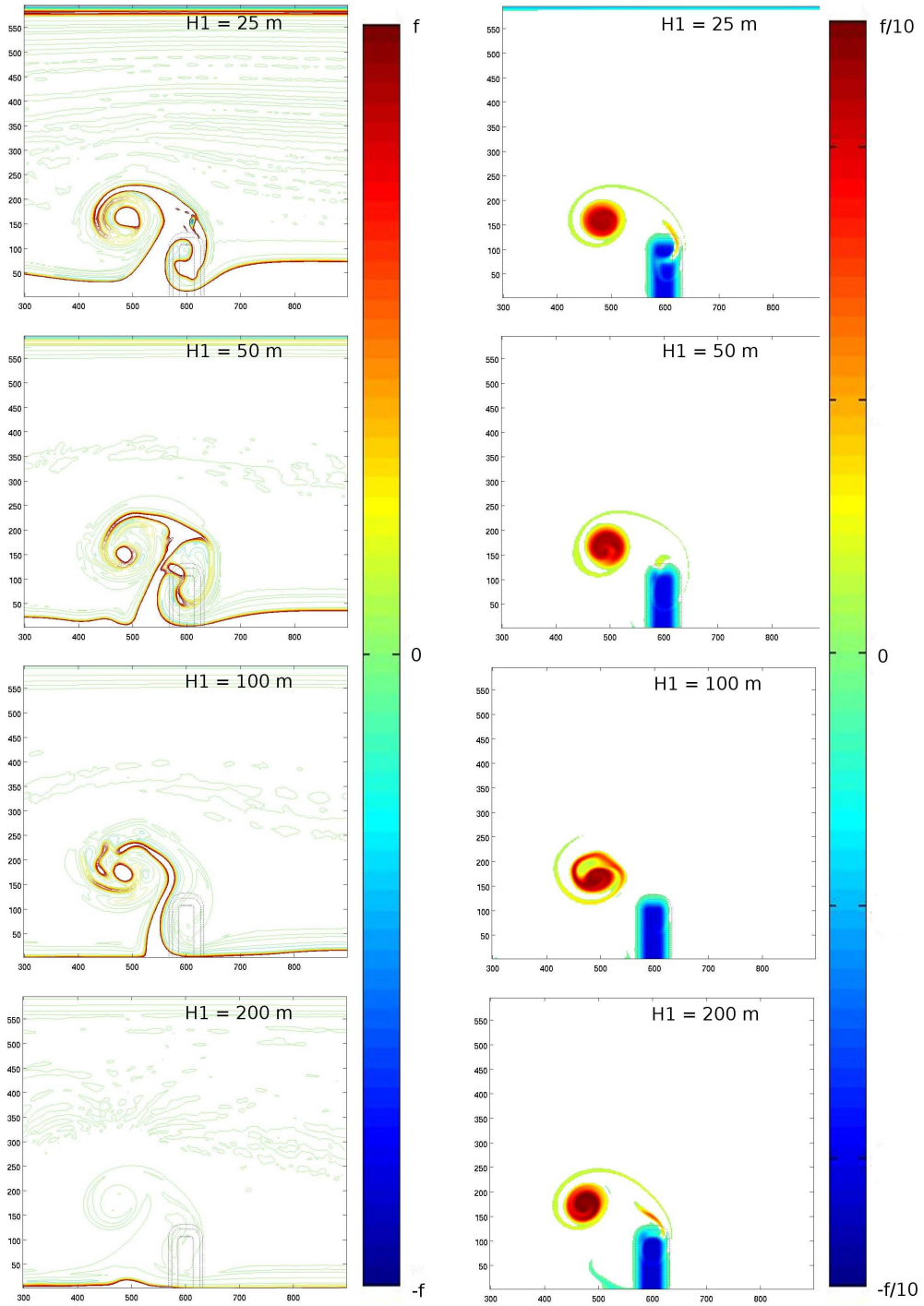


Figure 10: Maps of *PVA* in the upper (left hand panel) and bottom (right hand panel) layers at $t = 42$ days for the $H_1 = 25, 50, 100, 200$ m experiments.

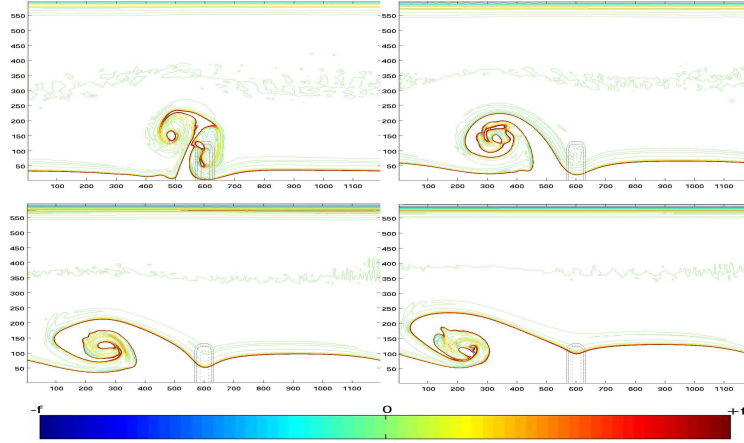


Figure 11: Maps of PVA in the upper layer at $t = 42$ days for the 10, 20, 30 and 40 days of wind forcing cases.

371 of the barotropic current.

372 Figure 11 shows the *PVA* front after 42 days of experiments in the upper layer for forcing
 373 durations of 10 (reference experiment), 20, 30, and 40 days. There still exists a trapped filament
 374 that extends far offshore downstream of the promontory, but its characteristics drastically depend
 375 on the forcing duration : it becomes thicker and bends downstream when the wind blows for a
 376 long time.

377 In fact, increasing the wind forcing duration does not substantially modify the formation of
 378 the *PVA* in the bottom layer but induces stronger barotropic current directed downstream. This
 379 intensified upwelling can mask the topographic circulation and the offshore jet. In addition, as
 380 the barotropic current increases, the positive pole becomes quickly advected downstream and
 381 only shortly interacts with the negative *PVA* pole on the topography. As a result, the upper
 382 layer *PVA* front rolls up cyclonically around the bottom layer positive *PVA* pole and is entrained
 383 downstream, giving it a breaking wave like shape. When increasing the forcing duration time, the
 384 distance from the front and jet to the coastal wall increases, while the offshore distortion of the
 385 front is less obvious, since its initial position almost reaches the offshore edge of the promontory
 386 (see the 40 day forcing case).

387 Notice that according to Eq. 13 and 15 the maximum barotropic velocity is roughly given
 388 by $U_b^{max} \simeq 8,6 \cdot 10^{-3} t_d$, where t_d is the duration time of the wind forcing in days. We thus get
 389 $U_b^{max} \simeq 8,6 \text{ cm/s}$ for 10 days and $U_b^{max} \simeq 34,4 \text{ cm/s}$ for 40 days, which is stronger than the
 390 offshore advection associated with the topographic eddies. Notice such barotropic currents are
 391 far beyond what is observed, at least offshore the continental shelf, and that in practice, bottom
 392 friction keeps the barotropic velocity from reaching such values.

393 4.4. The promontory height

394 As the main process proposed here for the development of an upwelling filament is the gen-
395 eration of topographic *PVA* in the bottom layer associated with the existence of a promontory,
396 it is important to detail how the shape and size of the latter can affect *PVA* generation and thus
397 filamentation. The maximum *PVA* and the strength of the topographic eddies are proportional to
398 the height of the promontory which is thus a key parameter.

399 Six experiments were carried out with different promontory heights : $H_t = 50, 100, 300, 500,$
400 1000 and 1500 m, to be compared with the 200 m of the reference experiment. Figure 12 shows
401 the upper and lower layer *PVA* field after 42 days for the $50, 200, 500,$ and 1500 m experiments.
402 For small topographies ($H_t = 50$ m), the filament forming in the upper layer along the front
403 has a much smaller offshore extension, is less pinched off and its tip is advected downstream.
404 In fact, the effect is the same as for the influence of the forcing duration discussed above: the
405 topographic circulation becomes much smaller than the upwelling current (the offshore current
406 is about 10 cm s^{-1} for $H_t = 50$ m, to be compared with the reference experiment where it is
407 about 40 cm s^{-1}). The positive *PV* pole is quickly advected downstream and the offshore current
408 is masked by the upwelling current giving the filament a breaking wave shape and limiting its
409 offshore extension.

410 The $H_t = 500$ and $H_t = 1500$ m experiments (see Fig. 12 left panels) show that after 42 days
411 of experiment, the filament is also much reduced in comparison with the reference experiment
412 (100 km for $H_t = 1500$ m, and 140 km for $H_t = 500$ m). The limiting factor for large H_t is
413 associated with the difficulty for water columns to climb on or leave the topography. Indeed,
414 most of the positive and negative *PVA* in the bottom layer remains trapped on the slope (see
415 Fig. 12 right panels). As a result, instead of forming two strong opposite sign *PVA* poles that
416 locally reinforce the offshore circulation, *PVA* of both signs mix on the promontory evolving
417 into a complex pattern of multiple small poles with few coherence. The overall integrated *PVA*
418 and circulation associated with the topographic eddies is then much reduced. In fact, as already
419 found by [Herbette et al., 2003] in the case of a vortex interaction with a seamount, the topo-
420 graphic circulation can not be much stronger than the background velocity and the *PVA* creation
421 is limited. Figure 13 shows the maximum extent of the filament for the 7 experiments. Similarly
422 to [Herbette et al., 2003]'s optimum value of seamount height for vortex erosion, there exists an
423 optimal promontory height for the filament extension which corresponds here to the reference
424 experiment : $H_t = 200$ m.

425 4.5. The promontory width

426 Three experiments were carried out to test the sensitivity of the filament formation to the width
427 of the promontory (parameter L_x). We tested $L_x = 0$ km (Gaussian ridge), 20 km (reference
428 experiment), $50,$ and 100 km (see Fig. 14). This parameter mostly affects the *PVA* reservoir and
429 strength of the circulation associated with the topographic eddies. The evolution of *PVA* in the
430 bottom layer for small L_x exhibits similarities with the reference experiment, with a generation
431 of negative *PVA* on the upstream part of the promontory in the first week of experiment, fully
432 invading it after 10 days, and a generation of positive *PVA* downstream of the ridge, quickly
433 evolving into a cyclonic vortex detaching from the offshore edge of the ridge. In fact, in the case
434 of small L_x , most of the *PVA* reservoir is contained along the promontory slope, not above the
435 plateau, and the results are then obviously not sensitive to this parameter in this case.

436 Increasing L_x increases the *PVA* reservoir and the potential strength of the topographic eddies.
437 The $L_x = 50$ km and 100 km cases show a strong rolling up of the positive *PVA* and of the filament

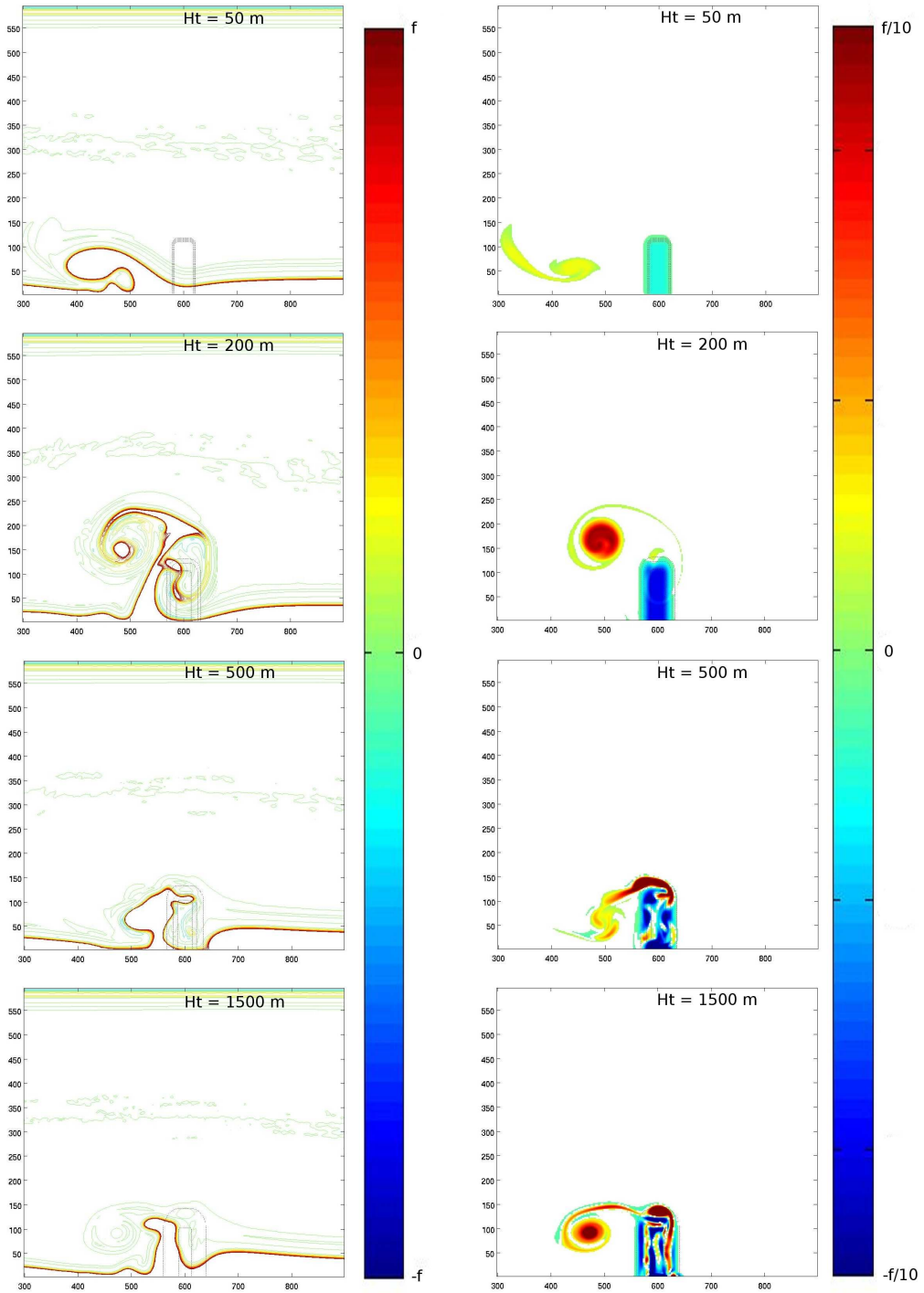


Figure 12: Maps of *PVA* in the upper (left hand panel) and bottom (right hand panel) layers at $t = 42$ days for the $H_t = 50, 200, 500$ and 1500 m experiments.

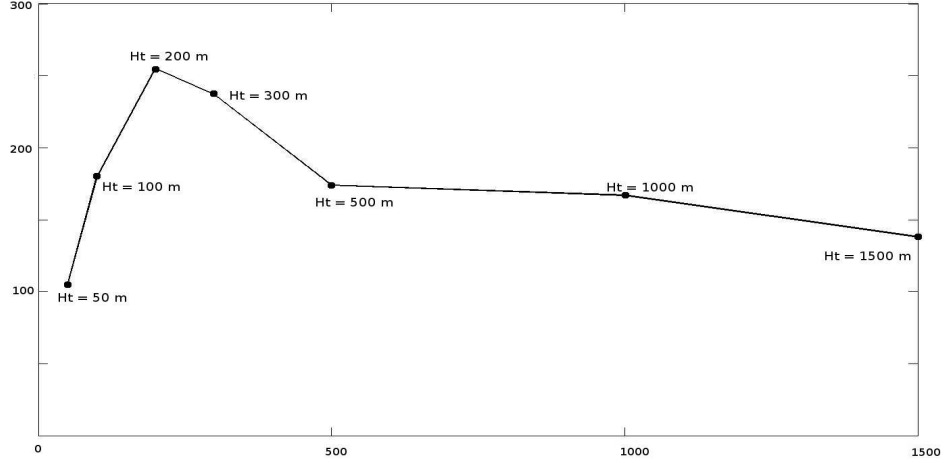


Figure 13: Offshore extent of the filament after 50 days of experiment for the $H_t = 50, 100, 200, 300, 500, 1000$ and $1500m$ cases. The x axis is H_t (kms) and the y axis is offshore distance (kms).

438 around the promontory. The *PVA* structure also exhibits a multipolar structure and the filament
 439 has multiple branches that do not extend very far offshore. In fact, strong topographic eddies
 440 leads to complex non linear interactions between the opposite sign *PVA* poles. The position
 441 and shape of the negative *PVA* is fixed and remains trapped above the promontory, whereas
 442 the positive one is advected and deformed by the total velocity field that develops in the lower
 443 layer. The latter effect is a combination between the barotropic circulation associated with the
 444 upwelling development, which is spatially constant, and the anticyclonic eddy, which varies
 445 spatially and can induce strong deformations. When the *PVA* reservoir increases, the effect of the
 446 negative *PVA* pole dominates the positive *PVA* pole and filament dynamics which are advected
 447 anticyclonically around the promontory and deformed. This greatly reduces the total length of
 448 the filament.

449 As a result, the width of the promontory also plays an important role in the development of
 450 a coherent filament structure in the upper layer and again, there exists an optimum value for
 451 the width of the promontory. This is shown in Fig. 15 where the offshore extension of the
 452 topographic filament is plotted for various choices of L_x . The optimum value is $L_x = 20$ km
 453 (reference experiment) for the present configuration.

454 4.6. The side slopes

455 In order to evaluate the importance of topographic β -effect in the offshore displacement of the
 456 positive *PVA*, three experiments were performed with different margin lengths for the promon-
 457 tory : $dL = 0, 10, 20$ (reference experiment) and 40 km. This parameter acts on the *PVA*
 458 reservoir (with close similarities with L_x) but also on the topographic slope and β -effect. The
 459 previous choices for dL corresponds to slopes $\tan\alpha = \infty, 2 \cdot 10^{-2}, 10^{-2}, 5 \cdot 10^{-3}$ respectively.

460 Figure 16 shows upper and lower layer *PVA* maps at $t = 42$ days for the different margin
 461 lengths. As could be expected, the influence of dL is similar to L_x : above a critical value,

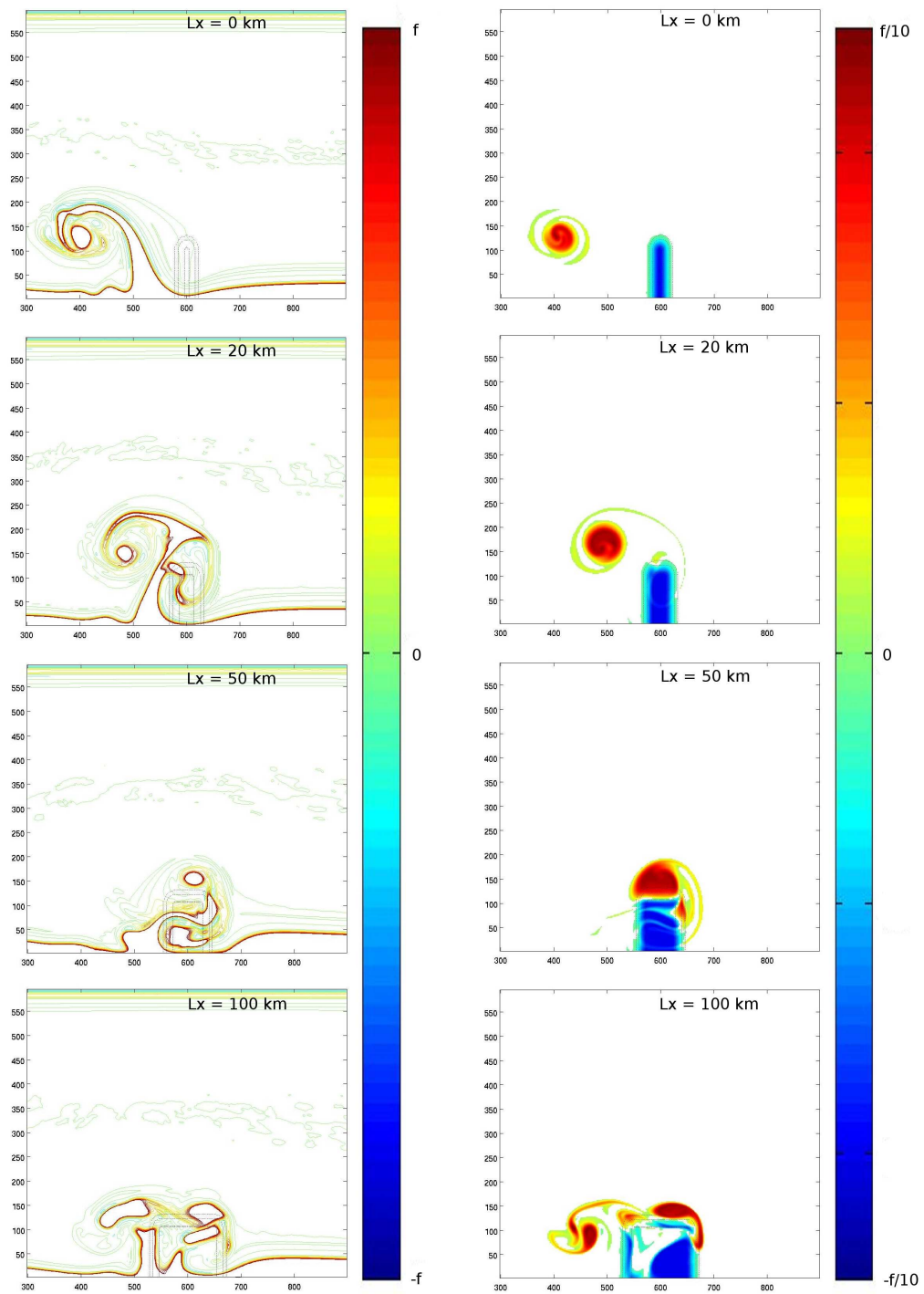


Figure 14: Maps of PVA in the upper (left hand panel) and bottom (right hand panel) layers at $t = 42$ days for the $L_x = 0, 20, 50$ and 100km experiments.

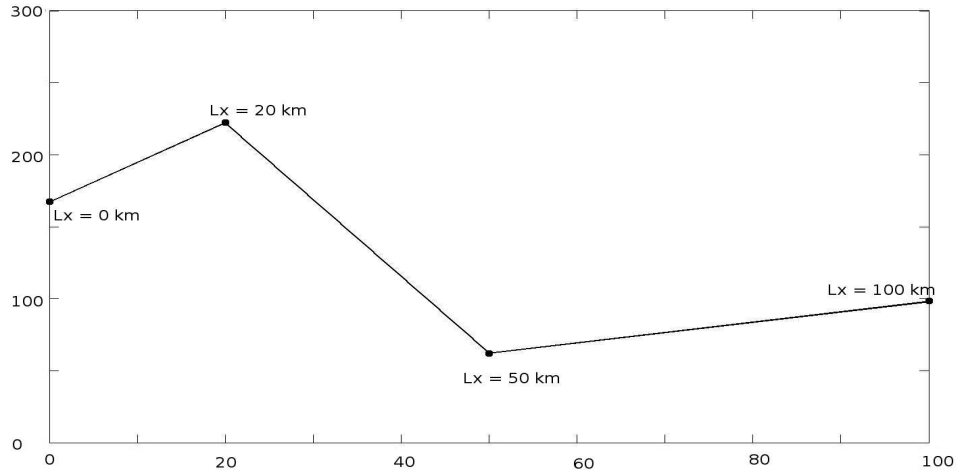


Figure 15: Offshore extent of the filament after 50 days of experiment for the $L_x = 0, 20, 50$ and 100km cases. The x axis is L_x (kms) and the y axis is offshore distance (kms).

462 the total circulation is dominated by the negative PVA pole and the filament wraps around the
 463 promontory. Despite very different values for the topographic slope and β -effect, the similarities
 464 between Fig. 16 and 14 are striking.

465 This confirms that the topographic β -effect has a minor impact on the dynamics, and that the
 466 important parameter in the generation of coherent and trapped filaments is the total amount of
 467 PVA over the promontory.

468 4.7. The promontory length

469 As discussed above, anisotropy in the shape of the promontory can also modify the structure
 470 and strength of the topographic circulation. The sensitivity of the results to the promontory length
 471 L_y was thus studied with $L_y = 50$ km, $L_y = 100$ km (reference experiment), $L_y = 150$ km and L_y
 472 $= 200$ km.

473 Figure 17 shows the structure of the PVA after 42 days in both layers and for the different
 474 L_y . The offshore extension of the bottom layer negative PVA pole obviously follows L_y and
 475 also drives the length of the filament which always extends further than the promontory. The
 476 $L_y = 200\text{km}$ case shows that there exists a maximum length of the filament over which it breaks,
 477 so that very long promontories are not necessarily the most efficient ones. This is underlined in
 478 Fig. 18 which shows the maximum offshore extension of the filament as a function of L_y . The
 479 optimal value is here around 150 km. Another particular feature for long promontories ($L_y = 200$
 480 km), is that the filament no longer rolls up around the positive PVA pole as it drifts far offshore,
 481 its base is much wider and its offshore shape much thinner.

482 4.8. Bottom friction

483 Two experiments were performed adding a bottom friction term to the reference configuration.
 484 Figure 19 shows the PVA in the upper layer (left hand panel) and the PV in the bottom layer at

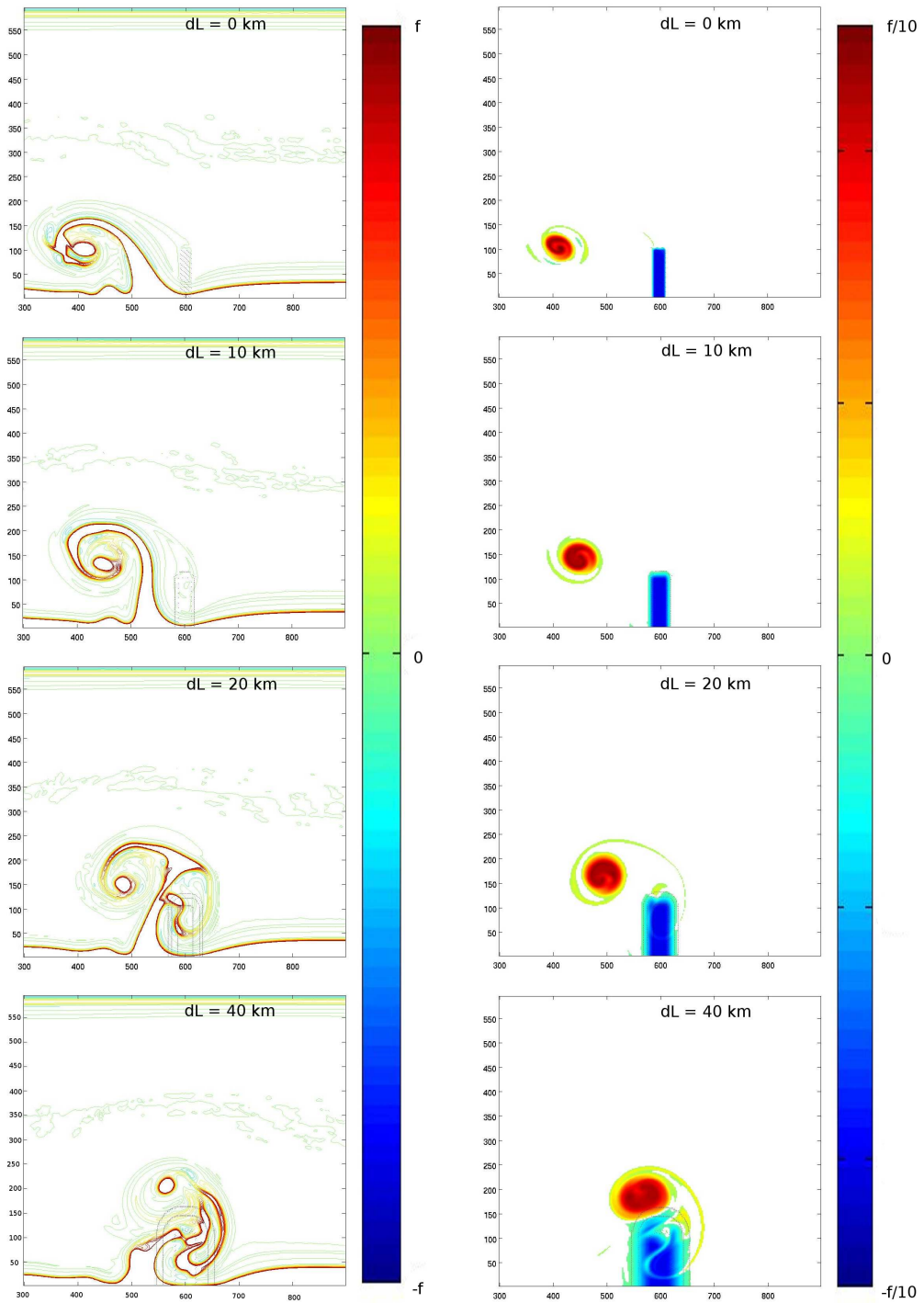


Figure 16: Maps of *PVA* in the upper (left hand panel) and bottom (right hand panel) layers at $t = 42$ days for the $dL = 0, 20, 50$ and 100km experiments.

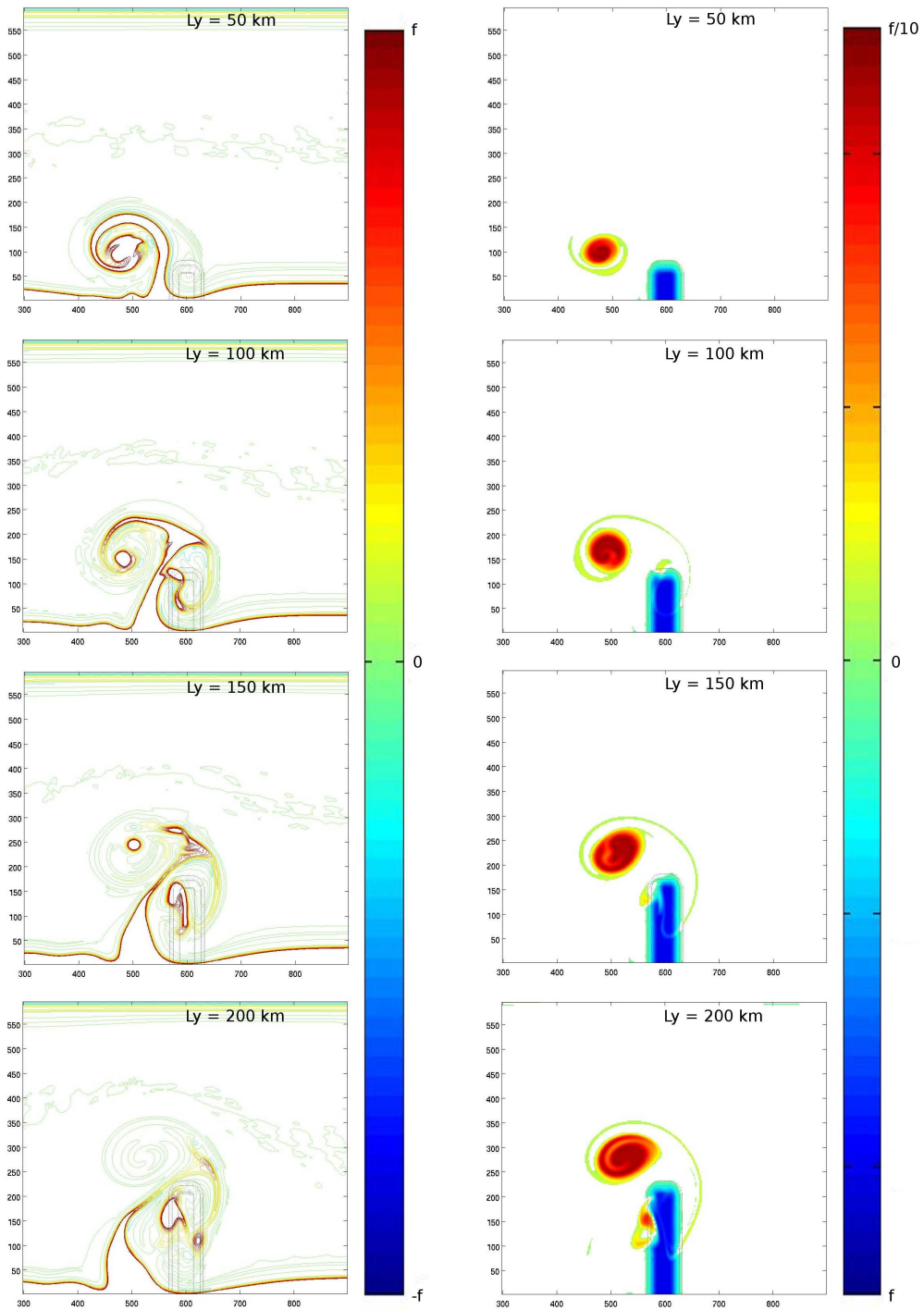


Figure 17: Maps of *PVA* in the upper (left hand panel) and bottom (right hand panel) layers at $t = 42$ days for the $Ly = 50, 100, 150$ and 200km experiments.

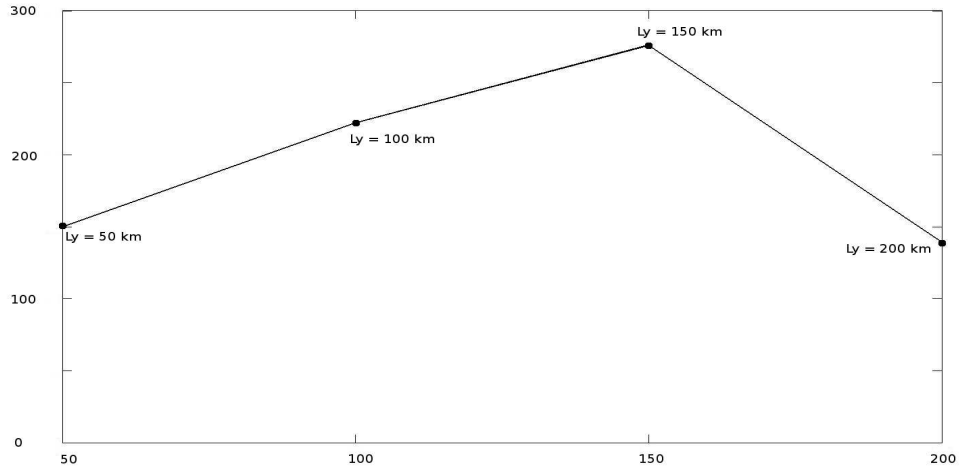


Figure 18: Offshore extent of the filament after 50 days of experiment for the $L_y = 50, 100, 150$ and 200km cases cases. The x axis is L_y (kms) and the y axis is offshore distance (kms).

485 $t = 42\text{days}$ (right hand panel) for the $C_d = 0, 3 \cdot 10^{-3}$, and $5 \cdot 10^{-3} \text{Nm}^{-2}$ cases. The formation
 486 and evolution of the filament in the upper layer is unchanged by the addition of the bottom
 487 friction. The effect of friction is only visible in the PV of the bottom layer: As the positive PV
 488 reservoir that has left the promontory to form the positive PVA pole gets eroded, new higher PV
 489 is generated over the promontory, resulting in weakening the negative PVA pole.

490 As a result, bottom friction leads to a relaxation of the circulation and to a new state of rest,
 491 which allows new topographic eddies and front filamentation to occur if the wind starts blowing
 492 again.

493 4.9. Influence of other topographic features

494 4.10. Capes

495 Complementary experiments including a cape or a cape superimposed on a larger promon-
 496 tory and a canyon where performed in order to compare the impact of the coastline geometry
 497 with the topographic process proposed here. Upwelling filament dynamics have sometimes been
 498 associated with capes triggering ([Strub *et al.*, 1991]), but most capes have large promontory-
 499 like undersea extends like Cabo Roca, Cabo Finisterre and the Estremadura promontory on the
 500 western Iberian coast.

501 The upper two panels in Fig. 20 show the PVA in the upper (left hand side) and bottom
 502 (right hand side) layer for two sizes of capes, both having the same Gaussian shape. Viscosity
 503 induces increased diabatic effects near boundaries which results here in the development of a
 504 layer of positive PVA . The presence of a cape allows this PVA to detach from the coast and
 505 wrap into a positive PVA pole. This process generates a cyclonic vortex downstream of the cape
 506 that in turn induces an offshore displacement of the outcropped front for small capes (cape 1
 507 is 50 km long and 25 km wide), and in the generation of a thin filament parallel to the coast

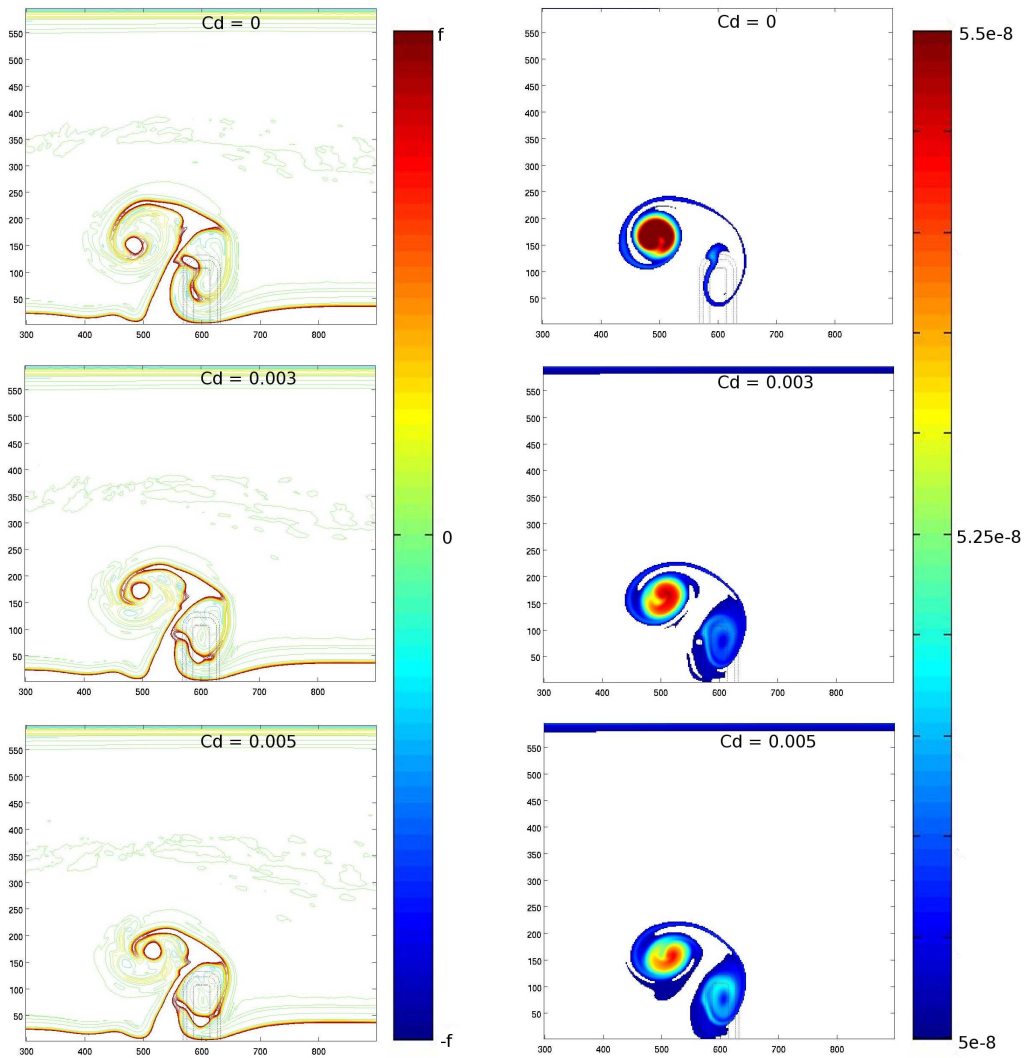


Figure 19: Maps of *PVA* in the upper (left hand panel) and bottom (right hand panel) layers at $t = 42$ days for the $C_d = 0, 3 \cdot 10^{-3}$ and $5 \cdot 10^{-3} \text{ Nm}^{-2}$ experiments.

508 for the larger capes (cape 2 is 100 km long and 100 km wide). Superimposing the first cape
509 with the reference promontory (third panel) leads to a long and thin filament pointing offshore
510 and developing downstream of the cape. This combination of cape and promontory seems to be
511 particularly efficient to generate the filament, because the cape alters the anticyclonic circulation
512 on the promontory, so that the filament keeps on growing offshore instead of rolling up around
513 the promontory.

514 4.11. Canyons

515 The lower panels in Fig. 20 show the effect of a canyon having the same shape as the reference
516 promontory. Such a configuration generates a cyclonic circulation above the promontory and an
517 anticyclonic one downstream. As a result, the jetlike current between both eddies is now directed
518 shoreward and can not generate a filament. However, the cyclonic circulation induces an offshore
519 current upstream of the canyon that, even though associated with a much weaker current than the
520 promontory case, can advect the upwelling front offshore. This is observed on Fig. 20 where a
521 filament forms in the upper layer upstream of the canyon. Also notice that the upwelling front
522 disappeared downstream of the promontory. There probably also exists an optimal shape of the
523 canyon for the development of the filament, but this is beyond the scope of the present study and
524 we simply conclude that canyons can also play an important role in the formation of trapped and
525 long upwelling filaments.

526 4.12. Combination of canyons and promontories

527 In many upwelling systems, the topography is not as simple as a promontory or a
528 canyon surrounded by a large flat bottom area. The bottom topography off the Rias Baixas, North
529 of the Iberian upwelling system is a good example of a succession of canyons and promontories.
530 In that case, a more complex dynamics is expected. To explore the impact of such a combi-
531 nation on the filament development and trapping, we set up two configurations : One with a
532 canyon downstream of the promontory and the other with a canyon upstream of the promon-
533 tory. Both are tested with two values of promontory/canyon height/depth. Figure 21 shows the
534 *PVA* in layer 1 (left hand side panels) and in layer 2 (right hand side panels) for a $H_t = 200m$
535 promontory/canyon combination (panel 1), $H_t = 100m$ promontory/canyon combination (panel
536 2), $H_t = 200m$ canyon/promontory combination (panel 3) and $H_t = 100m$ canyon/promontory
537 combination (panel 4). In all 4 cases, the bottom layer *PVA* dynamics is slightly complicated be-
538 cause of the generation of 4 *PVA* poles, but the main effects associated with the effect of isolated
539 topographic features are still visible : as the water initially situated over the flat bottom crosses
540 the promontory (canyon), a negative (positive) *PVA* is generated, while a positive (negative)
541 *PVA* is generated as the water from the promontory(canyon) crosses the canyon (promontory).
542 Another negative (positive) *PVA* is formed when the water originally located above the canyon
543 reaches the flat bottom area. Once the water columns originally situated upstream of the promon-
544 tory (canyon) have completely crossed the topography and reached the downstream flat bottom
545 area, the *PVA* distribution is as follow : 2 trapped opposite sign *PVA* over the promontory and
546 the canyon, and two free opposite sign *PVA* downstream of the topography, evolving as a dipole.
547 Note that in the $H_t = 200m$ cases, there is a slight multipolarisation because of stronger non
548 linear interaction between the higher *PVA* poles, while in the $H_t = 100m$ case, there is a stronger
549 advection of the free *PVA* poles.

550 Even though both canyon/promontory and promontory/canyon combinations produce long fil-
551 aments, there is a dynamical difference between them : In the promontory/canyon case, the most

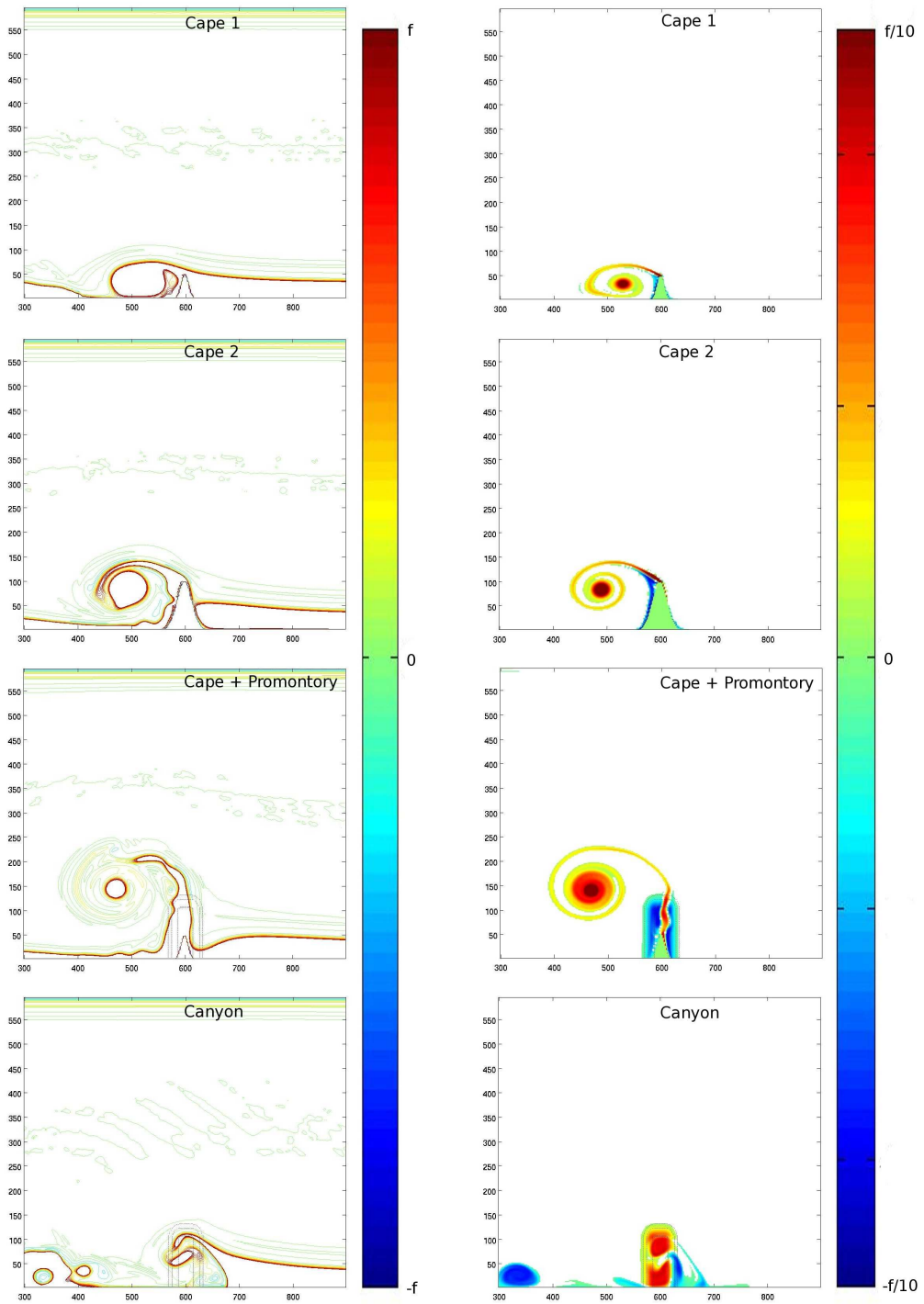


Figure 20: Maps of *PVA* in the upper (left hand panel) and bottom (right hand panel) layers at $t = 42$ days for the two capes experiments (panels 1 and 2), the cape over the promontory experiment (panel 3) and the canyon experiment (panel 4).

552 upstream *PVA* pole is the trapped negative one associated with the promontory which results
553 in an offshore deviation of the front, while in the canyon/promontory combination, the trapped
554 positive *PVA* associated with the canyon entrain the front inshore, inhibiting a proper filamen-
555 tation over the topography. This results in a major difference in the nature of the observed
556 filaments : while the filament of the promontory/canyon combination is generated by the effect
557 of the trapped dipole resulting in a permanently trapped filament between the promontory and
558 the canyon, the filament generated by the canyon/promontory combination is generated by the
559 effect of the free dipole resulting in a free filament, moving downstream as it gets advected by
560 the barotropic current.

561 As shown by these simple examples, the combinations of canyons and promontories with
562 complex shapes, as existing in nature, may lead to a more drastic selection of regions for the
563 generation of long and trapped filaments.!!!!?YM

564 **5. Conclusion**

565 *5.1. Generation of long trapped filament by topographic effect*

566 In this paper, we have studied the formation of long trapped upwelling filaments which are
567 ubiquitous features in all major upwelling systems. We focused on the effect of bottom topogra-
568 phy using an idealized two-layer configuration with a wind forcing that generates an upwelling
569 front along a vertical coastal wall in the presence of a transverse promontory or ridge. The phys-
570 ical process studied is based on the formation of *PVA* when the upwelling current interacts with
571 the bottom topography. At rest, in the bottom layer, the promontory is a positive potential vortic-
572 ity anomaly pool, because the ambient potential vorticity is stronger over the promontory than in
573 the rest of the domain. As the upwelling current sets up, this high potential vorticity gets advected
574 downstream of the promontory by the alongshore current, and is replaced by lower potential vortic-
575 ity water, generating a negative potential vorticity anomaly (*PVA*) over the promontory, and a
576 positive potential vorticity anomaly downstream. The positive *PVA* is advected offshore by the
577 trapped negative pole current field, and evolves into a cyclonic vortex eventually advected down-
578 stream. The negative *PVA* induces an anticyclonic circulation anomaly that remains trapped
579 above the topography and, if it is strong enough, will modify the mean upwelling current. This
580 produces a geostrophic offshore flow on the downstream side of the promontory which is able to
581 distort the upwelling front and then forms a meander. The latter finally evolves into a thin fila-
582 ments that grows offshore, and that may be sometimes slightly rolling up around the topographic
583 eddies. The barotropic part of the circulation plays the main role in the latter process.

584 Then, we evaluated the influence of baroclinic instability on the formation of the meanders
585 generated by topographic effects using stable and unstable configurations. The modelled stable
586 current is able to generate a very large and stationary filament when interacting with topog-
587 raphy whereas baroclinic instabilities of the jet produce additional numerous shorter me-
588 anders quickly propagating downstream that have a weak influence on the topographic fila-
589 ment development. The characteristics of the meanders and filaments associated with baro-
590 clinic instability are sensitive to the stratification and, as found in some previous studies (see
591 [*Haidvogel et al.*, 1991, *Strub et al.*, 1991]), long filament can also emerge in this case, but the
592 trapping of the filament and their development at identical locations can only be explained by
593 topographic effects.

594 We have also found that the deviation of the upwelling current by a cape and the generation of
595 vorticity by the viscous boundary layer generate a cyclonic pool of cold water downstream of the

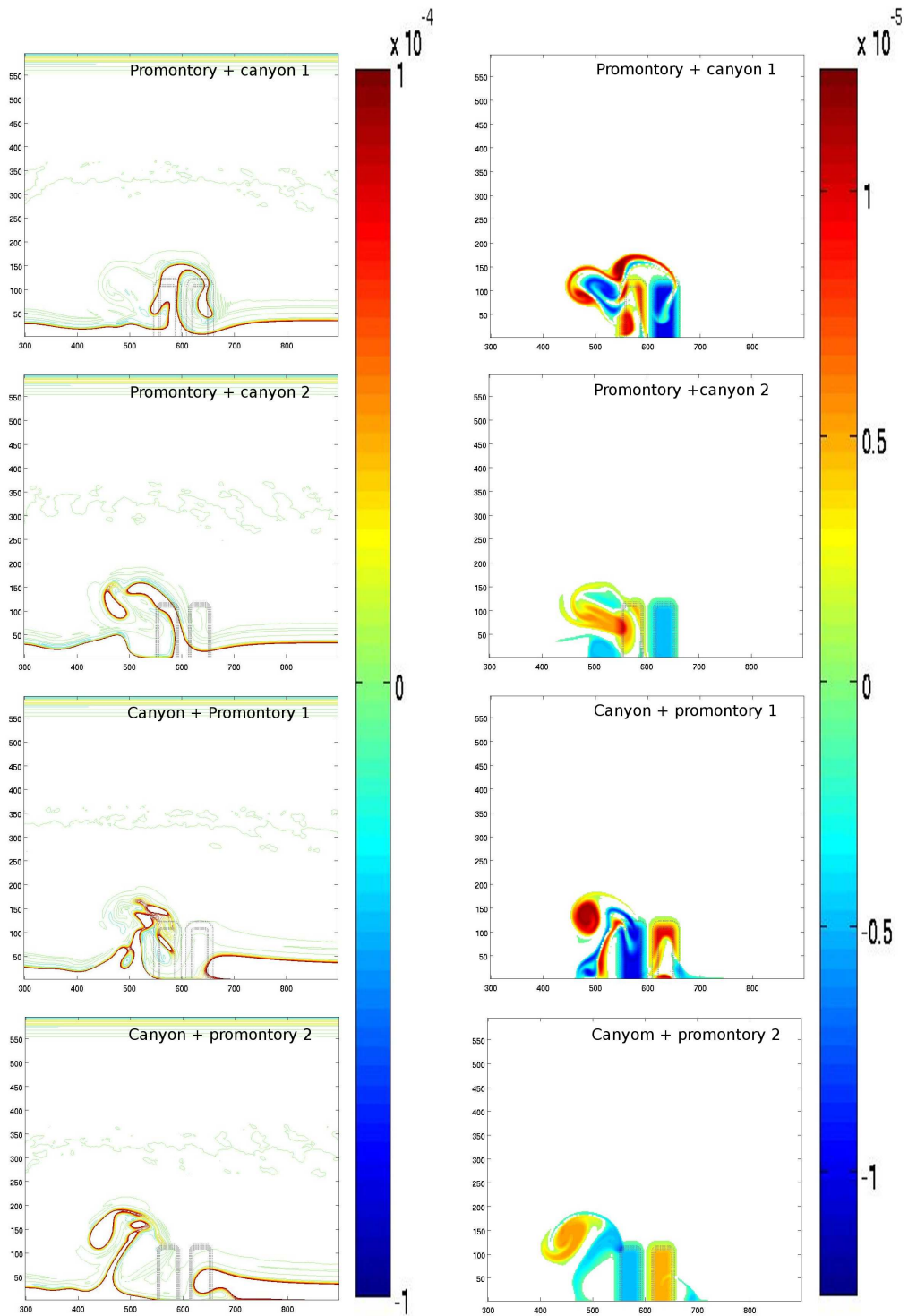


Figure 21: Maps of PVA in layer 1 (left hand side panels) and in layer 2 (right hand side panels) for a $H_t = 200m$ promontory/canyon combination (panel 1), $H_t = 100m$ promontory/canyon combination (panel 2), $H_t = 200m$ canyon/promontory combination (panel 3) and $H_t = 100m$ canyon/promontory combination (panel 4).

596 cape rather than a long offshore filament. Thus, at least for the simplified configurations used in
597 the present paper, the process involved in the generation of upwelling filaments at capes is rather
598 associated with the submarine promontories that generally exist in their continuity, modifying
599 the potential vorticity structure of the current as explained above.

600 The topographic eddies are generated by the barotropic circulation associated with the up-
601 welling development. Their advective effect on the upwelling front as well as the formation of
602 filaments are again associated with their barotropic vorticity. The process thus mainly involves
603 the barotropic circulation. As a consequence, modifying the stratification does not strongly mod-
604 ify the mechanism we have identified, nor the generation of topographic filaments as long as the
605 upwelling front is formed.

606 Increasing the duration of the wind forcing induces a further extension of the upwelling front,
607 and intensifies the strength of the upwelling barotropic current but not of the topographic ed-
608 dies. The cyclonic eddy detaching from the topography is thus advected further downstream
609 which, together with the change in the upwelling front extension, modify the characteristics of
610 the filament. In our case the filament width increases and bends downstream when applying
611 wind forcing for a longer time. Let us note that increasing the duration of the wind forcing also
612 increases the source of diabatic *PV* generation (see [Morel *et al.*, 2006]) and thus the instability
613 of the current. This was not investigated in the present paper, but we expect that, as a result, the
614 relative importance of the unstable structure increases as the forcing lasts longer, so that a greater
615 part of the offshore transport can be attributed to the instability of the jet in this case. This should
616 however not change our conclusions on the trapping of long upwelling filaments.

617 Sensitivity tests to the shape of the topographic feature have shown that the width, height,
618 length and slope of the topography are important parameters for the process. Multipolarisation
619 of the *PVA*, decreasing the coherence and the length of the surface filaments, can occur in the
620 case of a too wide or too tall promontory. The height of the promontory controls the available
621 *PVA* pool, so that a too small promontory can not produce a large stationary filament, but neither
622 can a very tall promontory above which flows and *PVA* can barely form. There exists optimal
623 values of the topography characteristics to maximize the offshore extension of the filament. In
624 other words, the formation of long trapped upwelling filaments by topographic features is a
625 selective process and is restricted to some height, width, slope and length ranges.

626 5.2. Discussion and perspectives

627 !!!!!YM Even though our model is of the simplest, it allows to clearly identify a dynamical
628 process which seems relevant to explain the stationarity and the repeatability of upwelling fila-
629 ments at some particular locations. This simplicity however makes a thorough comparison with
630 observed current structures a difficult task, but a qualitative discussion on some general patterns
631 remains possible.

632 It is important to note that the various upwelling systems develop over very different topogra-
633 phies : if the Iberian or the Chilean margins show complicated patterns with a succession of
634 ridges and canyons in the continuation of the rias, the North African topography is a combination
635 of a smooth margin with a few well defined promontories (Cape Ghir, Cape Blanc). As shown
636 in section 4.4 and 4.9, the generation of trapped filaments is highly sensitive to the topographic
637 configuration, and the multiplicity and greater variability of upwelling filaments along the West-
638 Iberian shelf could be explained by this more complex bottom topography. If the isolated Cape
639 Ghir promontory is a scholar case for the generation of well defined trapped anticyclone, trig-
640 gering a large long lived stationary filament, the multiple *PVA* poles generated over the complex
641 Iberian topography must lead to non-linear interactions, including fragmentation and merger of

642 the *PVA* poles leading to the observed shorter-lived, less coherent filament with higher spatial
643 and temporal variability.

644 ???YM ATTENTION, je pense que les conditions atmospheriques peuvent aussi pas mal jouer
645 : les vents sur la faade iberique sont assez inconstants et expliquent sans doute aussi pas mal la
646 variabilite observee. ???YM

647 Note also that the present study does not exclude the processes invoked by previous studies to
648 explain the generation of upwelling filaments. Indeed, topographically trapped eddies can com-
649 bine or interact with other filamentation processes. The Southern North-West African upwelling
650 system, offshore of Mauritania is a good example of the multiplicity of dynamics of the up-
651 welling filaments : Recent satellite and in-situ observations (SOLAS-ICON cruise, unpublished
652 yet) showed a whole range of filaments with different sizes, shapes and behaviour. The intrinsic
653 instability of the upwelling front generates pinched off meanders, developing and propagating all
654 along the front between the Arguin's bank and Cape Verde whereas a quasi permanent filament
655 associated with an anticyclonic eddy is found over the Cape Blanc promontory. Even though
656 this filament is quasi-permanently rooted over the Cap Blanc promontory, its offshore extension
657 shows a high spatial and temporal variability. This variability is believed to result from interac-
658 tions with an external mesoscale turbulence field resulting from the presence of the baroclinically
659 unstable Cape Verde front in the vicinity of the Mauritanian upwelling system. This confirms the
660 idea of [Strub *et al.*, 1991] that filaments could result of the combined effect of various processes
661 like jet instability and the interaction with an offshore eddy field. The role of bottom topography
662 is finally added to justify the stationarity and repeatability of filaments. ???YM ATTENTION: je
663 trouve que ce dernier paragraphe brouille le message. Il faut que le lecteur reparte avec comme
664 idee claire que jusqu' present seul le mecanisme propos ici permet d'expliquer la presence de long
665 filament pigs se developpant systmatiquement au mme endroit. D'autres mecanismes peuvent
666 soit gnrer des filaments (mais a priori ayant des caracteristiques en terme de stationnarite/pigeage
667 different) soit interagir avec le present effet pour en diminuer ou en augmenter les effets. Je suggere
668 de recrire ce paragraphe sur la base de ce fil conducteur. Tel quel ce paragraphe remet tout zro
669 mon sens : on comprend que finalement d'autre mecanisme peuvent trs bien expliquer le mme
670 comportement sans qu'on donne d'explication cela. ???YM

671 !!!??YM

672 The two-layer adiabatic model we have used is however very simplified and in nature, many
673 other parameters and many additional processes, that have not been studied here, can influence
674 the development of topographic eddies and formation of upwelling filaments, among which :

- 675 • the existence of an extended shelf and a continental slope ;
- 676 • the existence of a more complex and realistic large scale circulation (presence of a deep
677 poleward undercurrent) associated with or preceding the upwelling development;
- 678 • the influence of a more complicated stratification and of the specific dynamics of the mixed
679 layer or the influence of mixing in general;
- 680 • the influence of the planetary β effect;
- 681 • the influence of bottom friction.

682 The beta effect seems of particular importance as it strongly influences the dynamics of eddies
683 and induces westward propagation. We can thus imagine, for Eastern boundary upwellings,
684 that any localized source of vortices such as bottom topography, but also capes, could favor the

685 offshore development of filaments : indeed the cyclonic vortex developing downstream of a cape
686 would be advected westward entraining upwelled cold waters and forming a localized filament
687 instead of a circular patch as observed in the present study.

688 Another interesting subject is the influence of bottom friction. We have found here that its
689 influence was weak, but this was expected since we considered a deep ocean. Bottom friction
690 would obviously plays a stronger role than observed here for upwelling developing above shallow
691 areas (corresponding to extended shelves). As its effect is to reduce the currents in the bottom
692 layers, we expect this would limit the strength of the upwelling barotropic velocity and down-
693 stream transport. However, meanwhile it would also renew the reservoir of positive PVA above
694 the promontory. As a result, after a period of relaxation of the winds, despite the fact that the
695 initial positive PVA moved away from the topography, the same mechanism could be repeated
696 for a new upwelling event.

697 However, even though these processes can have a strong influences on the result and their effect
698 is worth investigating, we believe that they would not substantially modify our main result : the
699 bottom topography plays a key role on the formation of the long upwelling filaments, whatever
700 the direction of the current and details of the topography, PVA has to form when the flow passes
701 over topography, developing a trapped circulation whose signature extends over the entire water
702 column and influences the upper layer dynamics advecting water parcels offshore.

703 Finally, more in-situ observations of early stage development of upwelling filaments are
704 needed to possibly confirm our results and the main influence of the barotropic circulation associ-
705 ated with topographic eddies. This implies an extended mapping of the circulation, !!! including
706 the deep mesoscale features which are often neglected during the mesoscale surveys because of
707 the difficulty to sample at great depths without loosing time and thus synopticity. !!!

708 **6. Acknowledgements**

709 Part of this study has been conducted in the frame of the MOUTON project funded by DGA
710 (PEA 012401) and the CAIBEX project (CTM2007-66408-C02/MAR) funded by the Spanish
711 National government. T.M. thanks Pr E.D. Barton for the useful discussions and the calculation
712 time supplied at IIM-CSIC (Spain). V.R. is supported by a PhD grant from DGA. Satellite images
713 where provided by Joel Sudre at LEGOS.

714 **References**

- 715 [Alvarez-Salgado *et al.*, 2001] Alvarez-Salgado, X.A., M.D. Doval, A.V. Borges, I. Joint, M. Frankignoulle, E.M.S.
716 Woodward, F.G. Figueiras, Off-shelf fluxes of labile materials by an upwelling filament in the NW Iberian Up-
717 welling System. *Progress in Oceanography*, 51, 321-337, 2001.
- 718 [Alvarez-Salgado *et al.*, 2007] Alvarez-Salgado, X.A., Arstegui, J., Barton, E.D., Hansell, D.A., Contribution of up-
719 welling filaments to offshore carbon export in the subtropical Northeast Atlantic Ocean. *Limnology and Oceanog-*
720 *raphy*, 52, 1287-1292, 2007.
- 721 [Bang and Andrews, 1974] Bang, N.D., and Andrews, W.R.H., Direct current measurements of a shelf-edge frontal jet
722 in the southern Benguela system, *Journal of Marine Research*, 32, 407-421, 1974.
- 723 [Barth, 1989 a] Barth, J.A. Stability of a coastal upwelling front 1. Model developing and a stability theorem, *Journal*
724 *of Geophysical Research*, Vol. 94, 10844-10856, 1989.
- 725 [Barth, 1989 b] Barth, J.A. Stability of a coastal upwelling front 2. Model results and comparison with observations,
726 *Journal of Geophysical Research*, Vol. 94, 10857-10883., 1989.
- 727 [Barth, 1994] Barth, J.A. Short-wavelength instabilities on coastal jets and fronts, *Journal of Geophysical Research*,
728 Vol. 98, 16095-16115, 1994.
- 729 [Barton, 2001] Barton, E.D., M.E Inall, T.J, Sherwin and R. Torres., Vertical structure, turbulent mixing and fluxes
730 during Lagrangian observations of an upwelling filament system off Northwest Iberia, *Progress in Oceanography*,
731 Vol. 51, 249-267, 2001.
- 732 [Barton, 2004] Barton, E.D., Aristegui, J., Tett, T. and Navarro-Pérez, E., Variability in the Canary Islands Area of
733 Filament-Eddy Exchanges, *Progress in Oceanography*, Vol. 62, 71-94, 2004.
- 734 [Batteen, 1997] Batteen, M.L., Wind-forced modeling studies of currents, meanders, and eddies in the California Cur-
735 rent system *Journal of Geophysical Research-Oceans*, Vol 102, C1, 985-1010, 1997.
- 736 [Batteen *et al.*, 2007] Batteen, M.L., Martinho, A.S., Miller, H.A. and McClean, J.L., A Process-Oriented Study of the
737 Coastal Canary and Iberian Current System, *Ocean Modelling*, vol. 18, 1-36, 2007.
- 738 [Bleck and Boudra, 1986] Bleck., R. and Boudra, D., Wind driven spin-up in eddy-resolving ocean models formulated
739 in isopycnic and isobaric coordinates, *Journal of Geophysical Research*, vol. 91, 7611-7621, 1986.
- 740 [Bleck and Smith, 1990] Bleck., R. and Smith, L., A wind driven isopycnic coordinate model of the North and equatorial
741 Atlantic Ocean: Model development and supporting experiments *Journal of Geophysical Research*, vol. 95, 3273-
742 3285, 1990.
- 743 [Bleck *et al.*, 1992] Bleck., R., Rooth, C., Hu, D., and Smith, L., 1992. Salinity driven thermocline transients in a wind
744 and thermocline forced isopycnic coordinate model of the North Atlantic. *Journal of Physical Oceanography*, vol.
745 22, 1486-1505.
- 746 [Brink, 1983] Brink, K.H., The near-surface dynamics of coastal upwelling, *Progress in Oceanography*, vol. 12, 223-
747 257, 1983.
- 748 [Bretherton, 1966] Bretherton, F.P., Critical layer instability in baroclinic flows, *The Quarterly Journal of the Royal*
749 *Meteorological Society*, vol. 92, 325-334, 1966.
- 750 [Capet and Carton, 2004] Capet, X.J. and Carton, X.J. Nonlinear Regimes of Baroclinic Boundary Currents, *Journal*
751 *of Physical Oceanography*, vol. 34, 14001409, 2004.
- 752 [Charney and Stern, 1962] Charney, J.G. and Stern, M.E., On the Stability of Internal Baroclinic Jets in a Rotating
753 Atmosphere, *Journal of the Atmospheric Sciences*, vol. 19, 159172, 1962.
- 754 [Dewey *et al.*, 1991] Dewey, R.K., Moum, J.N., Paulson, C.A., Caldwell, D.R. and Pierce, S.D., Structure and Dynamics
755 of a Coastal Filament, *Journal of Geophysical Research*, vol. 96, 14885-14907, 1991.
- 756 [Flament *et al.*, 1985] Flament, P., Armi, L. and Washburn, L., The Evolving Structure of an Upwelling Filament,
757 *Journal of Geophysical Research*, vol. 90, 11765-11778, 1985.
- 758 [Garvine, 1971] Garvine, R.W., A simple model of coastal upwelling dynamics, *Journal of Physical Oceanography*, 1,
759 169-179, 1971.
- 760 [Garvine, 1973] Garvine, R.W., The effects of bathymetry on the coastal upwelling of homogeneous water, *Journal of*
761 *Physical Oceanography*, 3, 47-56, 1973.
- 762 [Gill and Clarke, 1974] Gill, A.E. and A.J., Clarke, Wind-induced upwelling, coastal currents and sea level changes,
763 *Deep-Sea Research*, vol. 21, 325-345, 1974.
- 764 [Haidvogel *et al.*, 1991] Haidvogel, D.B., Beckmann, A. and HedStrm, K.S., Dynamical Simulations of Filament For-
765 mation and Evolution in the Coastal Transition Zone, *Journal of Geophysical Research*, vol. 96, 15017-15040,
766 1991.
- 767 [Haynes *et al.*, 1993] Haynes, R., Barton, E.D. and Pilling, I. Development, Persistence, and Variability of Upwelling
768 Filaments, *Journal of Geophysical Research*, vol. 98, 22681-22692, 1993.
- 769 [Herbette *et al.*, 2003] Herbette, S., Morel, Y.G. and Arhan, M., Erosion of a surface vortex by a seamount, *Journal of*
770 *Physical Oceanography*, vol. 33, (8):1664-1679, 2003.

- 771 [Herbette *et al.*, 2005] Herbette, S., Morel, Y.G. and Arhan, M., Erosion of a surface vortex by a seamount on the beta
772 plane, *Journal of Physical Oceanography*, vol. 35, (11):2012-2030, 2005.
- 773 [Hoskins *et al.*, 1985] Hoskins, B., McIntyre, M. and W. Robertson, On the use and significance of isentropic potential
774 vorticity maps, *Quarterly Journal of the Royal Meteorological Society*, vol. 111, 877-946, 1985.
- 775 [Ikeda, 1981] Ikeda, M., Meanders and Detached Eddies of a Strong Eastward-Flowing Jet Using a Two-Layer Quai-
776 Geostrophic Model, *Journal of Physical Oceanography*, vol. 11, 526-540, 1981.
- 777 [Ikeda, 1989] Ikeda, M., Lygre, K. and Sandven, S., A Process Study of Mesoscale Meanders and Eddies in the Norwe-
778 gian Coastal Current, *Journal of Physical Oceanography*, vol. 19, 20-35 1989.
- 779 [Killworth, 1980] Killworth, P.D., Barotropic and baroclinic instability in rotating stratified fluids, *Dynamics of Atmo-*
780 *sphere and Ocean*, vol. 4, 143-184, 1980.
- 781 [Kostianoy and Zatsepin, 1996] Kostianoy, A.G. and Zatsepin, A.G., The West African coastal upwelling filaments and
782 cross-frontal water exchange conditioned by them, *Journal of Marine Systems*, vol. 7, 349-359, 1996.
- 783 [Lentz and Chapman, 2004] Lentz, S.J. and D.C., Chapman, The importance of nonlinear cross-shelf momentum flux
784 during wind-driven coastal upwelling, *Journal of Physical Oceanography*, 34, 2444-2457, 2004.
- 785 [Marchesiello *et al.*, 2003] Marchesiello, P., J. C. McWilliams and A. Shchepetkin, Equilibrium structure and dynam-
786 ics of the California Current System. *J. Phys. Oceanogr.*, 33, 753-783, 2003.
- 787 [McIntyre and Norton, 1990] McIntyre, M., and W. Norton, Dissipative wave-mean interactions and the transport of
788 vorticity or potential vorticity, *Journal of Fluid Mechanics*, vol. 212, 403-435, 1990.
- 789 [McWilliams and Gent, 1980] McWilliams, J.C., and Gent, P.R., 1980. Intermediate models of planetary circulations in
790 the atmosphere and the ocean. *Journal of Atmospheric Sciences*, vol. 37, 1657-1678.
- 791 [Morel and McWilliams, 2001] Morel, Y. and McWilliams, J., Effects of Isopycnal and Diapycnal Mixing on the Sta-
792 bility of Oceanic Currents, *Journal of Physical Oceanography*, vol. 31, 2280-2296, 2001.
- 793 [Morel *et al.*, 2006] Morel, Yves, G., Darr, D. S. and C. Talandier, Possible sources driving the Potential Vorticity struc-
794 ture and long-wave instability of coastal upwelling and downwelling currents *Journal of Physical Oceanography*,
795 vol. 36, 875-896, 2006.
- 796 [Morel and Thomas, 2009] Morel, Y. and Thomas, L.N., Ekman drift and vortical structures, *Ocean modelling*, vol. 27,
797 185-197, 2009.
- 798 [Navarro-Pérez and Barton, 1998] Navarro-Pérez, E. and Barton, E.D., The Physical Structure of an Upwelling Fil-
799 ament off the North-West African Coast during August 1993, *South African Journal of Marine Science*, vol. 19,
800 61-73, 1998.
- 801 [O'Brien and Hurlburt, 1972] O'Brien, J.J. and Hurlburt, H.E., A numerical model of coastal upwelling, *Journal of*
802 *Physical Oceanography*, vol. 2, 1972.
- 803 [Pringle, 2002] Pringle, J.M., Enhancement of wind-driven Upwelling and Downwelling by alongshore bathymetric
804 variability, *Journal of Physical Oceanography*, 32, 3101-3112, 2002.
- 805 [Relvas *et al.*, 2007] Relvas, P., Barton, E.D., Dubert, J., Oliveira, P.B., Peliz, A., da Silva, J.C.B. and A.M.P. Santos,
806 Physical oceanography of the western Iberia ecosystem: Latest views and challenges, *Progress in Oceanography*,
807 74, 149-173, 2007.
- 808 [Rossi *et al.*, 2009] Rossi, V., Morel, Y. and Garçon, V., Effect of the wind on the shelf dynamics: Formation of a
809 secondary upwelling along the continental margin, *Ocean Modelling*, 2009, doi : 10.1016/j.ocemod.2009.10.002.
- 810 [Roed and Shi, 1999] Roed, L. P., and X. B. Shi, A numerical study of the dynamics and energetics of cool filaments,
811 jets and eddies off the Iberian Peninsula. *Journal of Geophysical Research*, 104(C12), 29817-29841, 1999.
- 812 [Sanchez *et al.*, 2008] R. F. Sanchez, P. Relvas, A. Martinho, and P. Miller, Physical description of an upwelling fil-
813 ament west of Cape St. Vincent in late October 2004, *Journal of Geophysical Research*, Vol. 113, C07044,
814 doi:10.1029/2007JC004430, 2008.
- 815 [Shi and Roed, 1999] X. B. Shi and Roed, L. P., Frontal Instabilities in a Two-Layer, Primitive Equation Ocean Model,
816 *Journal of Physical Oceanography*, Vol. 29, 948-968, 1999.
- 817 [Stern and Chassignet, 2000] M.E. Stern and E.P. Chassignet, Mechanism of eddy separation from coastal currents ,
818 *Journal of Marine Research*, Vol. 58, 269-295, 2000.
- 819 [Strub *et al.*, 1991] Strub, T.P., Kosro, P.M., and Huyer, A., The nature of the cold filaments in the California Current
820 System, *Journal of Geophysical Research*, vol. 96, 14743-14768, 1991.
- 821 [Thomas, 2005] Thomas, L.N., Destruction of potential vorticity by winds, *J. Phys. Ocean.*, vol. 35, 2457-2466, 2005.
- 822 [Verron and Le Provost, 1985] Verron, J. and Le Provost, C., A numerical study of quasi-geostrophic flow over topog-
823 raphy, *J. Fluid Mech.*, vol. 154, 231-252, 1985.
- 824 [Viera and Grimshaw, 1994] Viera, F. and Grimshaw, R., Topographic Forcing of Coastal Mesoscale Phenomena: Fil-
825 amentation, Vortex Formation, and Eddy Detachment, *Journal of Physical Oceanography*, vol. 24, 1433-1448,
826 1994.
- 827 [Washburn and Armi, 1988] Washburn, L. and Armi, L., Observations of Frontal Instabilities on an Upwelling Filament,
828 *Journal of Physical Oceanography*, vol. 18, 1075-1092, 1988.
- 829 [Winther *et al.*, 2007] Winther, N.G., Morel, Y.G. and Evensen, G., Efficiency of high order numerical schemes for

δt_t	δt_c	δx	N_x	N_y	N_{days}	ν	T_x	f	$H_2 + H_1$
5 s	200 s	2000 m	601 pts	301 pts	50 days	$0.3 \text{ m}^2 \text{ s}^{-1}$	-0.2 Nm^{-2}	10^{-4} s^{-1}	2050 m

Table 1: Table of the model parameters kept fixed in all experiments.

Experiment	$d\rho \text{ (kgm}^{-3}\text{)}$	Cd	$H_1 \text{ (m)}$	Forcing duration (days)	$H_t \text{ (m)}$	$L_x \text{ (km)}$	$L_y \text{ (km)}$	$dL \text{ (km)}$
Ref	1	0	50	10	200	20	100	20
Inst	1	0	50	10	200	20	100	20
Notopo frc 10	1	0	50	10	<u>0</u>	<u>0</u>	<u>0</u>	<u>0</u>
Notopo frc 20	1	0	50	<u>20</u>	<u>0</u>	<u>0</u>	<u>0</u>	<u>0</u>
Notopo frc 30	1	0	50	<u>30</u>	<u>0</u>	<u>0</u>	<u>0</u>	<u>0</u>
Notopo frc 40	1	0	50	<u>40</u>	<u>0</u>	<u>0</u>	<u>0</u>	<u>0</u>
Cd 3e-3	1	<u>$3 \cdot 10^{-3}$</u>	50	10	200	20	100	20
Cd 5 e-3	1	<u>$5 \cdot 10^{-3}$</u>	50	10	200	20	100	20
frc time 20	1	0	50	20	200	20	100	20
frc time 30	1	0	50	30	200	20	100	20
frc time 40	1	0	50	40	200	20	100	20
H_t 50	1	0	50	10	<u>50</u>	20	100	20
H_t 100	1	0	50	10	<u>100</u>	20	100	20
H_t 300	1	0	50	10	<u>300</u>	20	100	20
H_t 500	1	0	50	10	<u>500</u>	20	100	20
H_t 1000	1	0	50	10	<u>1000</u>	20	100	20
H_t 1500	1	0	50	10	<u>1500</u>	20	100	20
L_x 0	1	0	50	10	200	<u>0</u>	100	20
L_x 50	1	0	50	10	200	<u>50</u>	100	20
L_x 100	1	0	50	10	200	<u>100</u>	100	20
L_y 50	1	0	50	10	200	20	<u>50</u>	20
L_y 150	1	0	50	10	200	20	<u>150</u>	20
L_y 200	1	0	50	10	200	20	<u>200</u>	20
dL 0	1	0	50	10	200	20	100	<u>0</u>
dL 10	1	0	50	10	200	20	100	<u>10</u>
dL 40	1	0	50	10	200	20	100	<u>40</u>
H_1 25	1	0	<u>25</u>	10	200	20	100	20
H_1 100	1	0	<u>100</u>	10	200	20	100	20
H_1 200	1	0	<u>200</u>	10	200	20	100	20
$d\rho$ 0.5	<u>0.5</u>	0	50	10	200	20	100	20
$d\rho$ 2	<u>2</u>	0	50	10	200	20	100	20
$d\rho$ 3	3	0	50	10	200	20	100	20

Table 2: Table of the model parameters that were varied in the various experiments.